NOVA SCHOOL OF SCIENCE & TECHNOLOGY

DEPARTMENT OF PHYSICS

MATILDE DE VASCONCELOS CARDOSO

Bachelor of Science in Biomedical Engineering

PHASE-AMPLITUDE COUPLING BETWEEN SLOW AND HIGH FREQUENCY EEG OSCILLATIONS AFTER PERIPHERAL NERVE STIMULATION IN HUMANS

MASTER IN BIOMEDICAL ENGINEERING

NOVA University Lisbon
September, 2024

NOVA SCHOOL OF
SCIENCE & TECHNOLOGY

DEPARTMENT OF
PHYSICS

PHASE-AMPLITUDE COUPLING BETWEEN SLOW AND HIGH FREQUENCY EEG OSCILLATIONS AFTER PERIPHERAL NERVE STIMULATION IN HUMANS

MATILDE DE VASCONCELOS CARDOSO

Bachelor of Science in Biomedical Engineering

Adviser: Véronique Marchand-Pauvert
Research Director, LIB, Sorbonne University

Co-adviser: Carla Quintão Pereira
Assistant Professor, NOVA University Lisbon

Examination Committee

Chair: Célia Maria Reis Henriques
Associate Professor, NOVA University Lisbon

Rapporteur: Alexandre da Rocha Freire de Andrade
Assistant Professor, University of Lisbon

Adviser: Véronique Marchand-Pauvert
Research Director, LIB, Sorbonne University

MASTER IN BIOMEDICAL ENGINEERING

NOVA University Lisbon
September, 2024

Phase-amplitude coupling between slow and high frequency EEG oscillations after peripheral nerve stimulation in humans

Copyright © Matilde de Vasconcelos Cardoso, NOVA School of Science and Technology, NOVA University Lisbon.
The NOVA School of Science and Technology and the NOVA University Lisbon have the right, perpetual and without geographical boundaries, to file and publish this dissertation through printed copies reproduced on paper or on digital form, or by any other means known or that may be invented, and to disseminate through scientific repositories and admit its copying and distribution for non-commercial, educational or research purposes, as long as credit is given to the author and editor.

This document was created with the (pdf/Xe/Lua)LaTeX processor and the NOVAthesis template (v7.1.27) [1].

To my beloved family, past and present,
with all my heart.

Acknowledgements

For the time being, this endeavour symbolises the final milestone of my academic journey, of which, whatever happens, I am deeply proud of. Hence, I have only gratitude to express to all those who, one way or another, contributed to the realisation of this work.

First and foremost, my profound thanks to my adviser Véronique Marchand-Pauvert, PhD, from the Neural Connectivity and Plasticity team of Laboratoire d'Imagerie Biomédicale at Sorbonne Université, who opened the door for me to take on a project at this institution, place that was home for six months. Your availability, kindness, and problem management taught me that the pursuit of science should be faced with pliability, paving the way for better resolutions. To Alper, PhD student, my co-adviser (and friend), thank you for guiding me through all the ups and downs. Your good mood, even during Parisian gray weather, spared me a few headaches. To Guillaume, PhD, you have my deepest gratitude for your advice, expertise, and support.

I extend my gratitude to all my laboratory colleagues for your company and for welcoming me so well. To Gaïa, you were the best deskmate I could have gotten. Thank you for introducing me to french slang and improving my daily steps. Xiomara, you are one of the kindest souls I have ever met, and I am glad I got the chance to be your flower girl. You two made my stay in Paris joyful, not only for making it easier to go to work every day, but also due to our flan pursue; I will cherish you both for life.

I also wish to extend my gratitude to NOVA School of Science and Technology and all the professors who played not only their role as teachers but also as mentors. To my co-adviser, Prof. Carla Quintão, I offer my utmost appreciation. Your assistance and heartfelt dedication to your students throughout the last five years were truly special.

From the very first day I stepped foot in FCT, I knew I had gained a second family, greater than just group studies or *jantares de curso*. To all who I crossed paths with and grew alongside me as the years passed, you ensured my journey was complete. From "All the flowers" in Oulu to all the "Avecs" in Paris, you put a smile on my face even in the grayest of days. To Duarte, thank you for your kindness at any moment. To my "descendants", António, Lili, and Janine, thank you for trusting in me. To Toni, thank you for showing me it is never too late to be special to someone. To all my *Matildes, Catarinas*

& Co., my heartfelt appreciation goes to you. Antão and Matela, my gratitude for our friendship is endless. It was hard, but without you it would have been even harder, with fewer laughs, *minis*, and probably fewer *pulos de galo*. I am sure you will go far, and I cannot wait to witness it.

To the people who are dearest to my heart: please know that without you, none of this would have been possible. To my parents and sister, who always supported me even when I was 5000 km away from home, thank you for all the lessons, all the help, and for giving me the freedom to become the woman I am today. Your encouragement, your caring words, and our shared adventures impacted me more than what you imagine. To my grandparents, I love you for everything you gave me, but I love you even more for what you gave to our family. To Conceição, your presence in my life showed me what true affection is like, and I thank you for raising me as one of your own.

To Nicolas, you are the best friend and partner I could have asked for. For your help in stressful times and for providing me with unwavering emotional support, your company was invaluable. Thank you for sharing life with me, wherever we might be.

Abstract

Amyotrophic Lateral Sclerosis (ALS) is a complex neurodegenerative syndrome affecting upper and lower motor neurons (UMN and LMN, respectively). Current diagnosis relies on evidence of simultaneous brain and spinal motor neuron degeneration, which is often imprecise due to the clinical challenge of recognising cortical dysfunctions. Muscle atrophy from LMN degeneration, frequently masks UMN symptoms, complicating the diagnosis and delaying treatment initiation.

Transcranial Magnetic Stimulation (TMS) studies have identified an imbalanced excitation/inhibition (E/I) ratio in the early stages of ALS, indicating motor cortex hyperexcitability even before symptoms appear. However, this method is unreliable with disease progression, emphasizing the need for biomarkers that can consistently track cortical dysfunctions in order to enhance ALS diagnosis. It has been shown that theta-gamma phase-amplitude coupling (PAC) extracted from resting state electroencephalography (EEG) can serve as a neuromarker of early cortical dysfunctions in ALS. This suggests that EEG analysis, especially through PAC, can break new ground.

The present study further explores beta-gamma PAC after peripheral nerve stimulation as a potential early biomarker for cortical dysfunctions in ALS. By exploring the effects of applied stimuli, the aim is to uncover valuable insights into disease evaluation, presenting a departure from previous approaches and methodologies. Coupling mean modulation index (MI) was assessed to estimate PAC between slow signals within the beta band (12-30 Hz), and higher frequency oscillations within the gamma band (30-100 Hz), at the level of 12 channels covering the sensorimotor cortex of both hemispheres. Results from linear mixed models show no significant differences between healthy and ALS patients, indicating that, through this method, a biomarker for early stage ALS disease cannot be detected in stimulated data.

Keywords: ALS, cortical dysfunctions, biomarker, EEG, PAC

Resumo

A Esclerose Lateral Amiotrófica (ELA) é uma síndrome neurodegenerativa complexa que afeta os neurónios motores superiores (NMS) e inferiores (NMI). O diagnóstico atual baseia-se na evidência de degeneração simultânea dos neurónios motores cerebrais e espinais, o que é muitas vezes complicado devido ao desafio clínico de reconhecer as disfunções corticais. A atrofia muscular resultante da degenerescência dos NMI camufla frequentemente os sintomas dos NMS, complicando o diagnóstico e atrasando o início do tratamento.

Alguns estudos de Estimulação Magnética Transcraniana (EMT) identificaram um desequilíbrio na relação excitação/inibição (E/I) nas fases iniciais da ELA, indicando uma hiperexcitabilidade do córtex motor mesmo antes do aparecimento dos sintomas. No entanto, este método não é fiável com a progressão da doença, enfatizando a necessidade de biomarcadores que possam rastrear consistentemente as disfunções corticais, a fim de melhorar o diagnóstico da ELA. Já foi demonstrado que o acoplamento fase-amplitude (AFA) theta-gamma extraído de dados de eletroencefalografia (EEG) em estado de repouso pode servir como um neuromarcador precoce de disfunções corticais na ELA. Isto sugere que a análise de EEG, especialmente através do AFA, pode abrir novos caminhos.

O presente estudo explora ainda mais o AFA beta-gamma após estimulação do nervo periférico como um potencial biomarcador precoce para disfunções corticais na ELA. Ao explorar os efeitos dos estímulos aplicados, o objetivo é descobrir informações valiosas sobre a avaliação da doença, apresentando um desvio em relação a abordagens e metodologias anteriores. O índice de modulação (IM) médio do acoplamento foi avaliado para estimar o AFA entre sinais lentos na banda beta (12-30 Hz) e oscilações de frequência mais elevada na banda gamma (30-100 Hz), ao nível de 12 canais que cobrem o córtex sensório-motor de ambos os hemisférios. Contudo, os resultados dos modelos lineares mistos não mostram diferenças significativas entre os sujeitos saudáveis e os doentes com ELA, indicando que não é possível detetar um biomarcador para a fase inicial da doença nos dados estimulados, adotando este método.

Palavras-chave: ELA, disfunções corticais, biomarcador, EEG, AFA

Contents

List of Figures **xv**

List of Tables **xvii**

Acronyms **xix**

1 Introduction **1**
1.1 Context and Motivation 1
1.2 Objectives 3
1.3 Thesis outline 4

2 Concepts **7**
2.1 Excitation/Inhibition Balance 7
2.2 Cortical Hyperexcitability 7
2.3 Electroencephalography 8
2.4 Somatosensory Evoked Potentials 8
2.5 Neuronal oscillations 9
2.6 Phase-Amplitude Coupling 10
2.7 Modulation Index 11
2.8 Comodulogram 11

3 State of the Art **13**
3.1 Cortical excitability in ALS 13
3.1.1 Transcranial Magnetic Stimulation 13
3.1.2 Functional Magnetic Resonance Imaging 13
3.2 Phase-Amplitude Coupling 14
3.2.1 PAC dependence on cortical excitability 14
3.2.2 PAC alterations in neurodegenerative diseases 14
3.2.3 PAC limitations and assessment 14
3.2.4 PAC preliminary results in ALS 15

4 Methods **17**
4.1 Data acquisition . . . 17
4.2 Experimental protocol . . . 18
4.3 EEG preprocessing . . . 20
4.4 PAC analysis . . . 21
4.4.1 Adaptation of the existing pipeline . . . 22
4.4.2 Surrogate data problematic . . . 22
4.4.3 *pactools* approach . . . 23
4.5 Statistical analysis . . . 23

5 Results and Discussion **27**
5.1 Surrogate data production . . . 27
5.1.1 Circular shifting . . . 27
5.1.2 Randomised trial shuffling . . . 27
5.1.3 Section discussion . . . 28
5.2 Statistical analysis of PAC . . . 29
5.2.1 rmLMM for mean MI considering two runs . . . 29
5.2.2 rmLMM for mean MI considering the average of runs . . . 30
5.2.3 rmLMM for mean z-score in two runs . . . 32
5.2.4 rmLMM for mean z-score with average of runs . . . 33
5.2.5 Section discussion . . . 34

6 Conclusions **37**
6.1 Main conclusions . . . 37
6.2 Limitations . . . 38
6.3 Future work . . . 38

Bibliography **41**

Appendices

A EEG preprocessing stages **47**
A.1 Raw signal . . . 47
A.2 Filtering . . . 48
A.3 Resampling . . . 49
A.4 Bad channels . . . 49
A.5 Re-referencing . . . 51
A.6 ICA . . . 52
A.7 Bad segments . . . 55
A.8 Epochs . . . 56

B Preprocessing filters' frequencies **57**
B.1 Data spectrum analysis . . . 57

B.2 Time frequency analysis 58

C MI calculus steps **61**

D Linear Mixed model specifications **63**

List of Figures

1.1 The Motor System. 2

2.1 N9 and N20 amplitude. 9
2.2 phase-amplitude coupling (PAC) - Gamma amplitude modulated by theta phase. 10
2.3 Comodulogram: example of PAC intensity. 12

3.1 Five central electrodes placed in the scalp. 15

4.1 74 channels electroencephalography (EEG) brain cap. 18
4.2 Representation of the stimulation applied in each subject. 19
4.3 Preprocessing pipeline. 20
4.4 Brain's average response. 21
4.5 Channels of interest. 24
4.6 Data distribution. 25

5.1 Example of autocorrelation of the high-frequency amplitudes envelope. . . 28
5.2 Example of a correlation matrix of high-frequency amplitudes envelope. . . 29
5.3 least square means (LSMeans) plot comparing the effects of Group, Channel, and Run. 30
5.4 receiver operating characteristic (ROC) curve for Cz channel. 31
5.5 The averaged mean Modulation Index (MI) values are plotted against the effects of Group and Channel using an LSMeans plot. 32
5.6 ROC curve for Cz channel. 33
5.7 LSMeans plot comparing the effects of Group, Channel, and Run. 34
5.8 The averaged mean z-scores are plotted against the effects of Group and Channel using an LSMeans plot. 35

A.1 Plot of the raw EEG signals. 47
A.2 Plot of the EEG signals after filtering. 48
A.3 Plot of the EEG signals after resampling. 49

A.4 Plot of the EEG signals after bad channels. 50
A.5 Plot of the EEG signals after interpolation of bad channels. 50
A.6 Plot of the EEG signals after re-referencing. 51
A.7 Plot of the 20 first independent component analysis (ICA) components. . . . 52
A.8 Plot of the 20 first ICA components topographic maps. 53
A.9 ICA artefact components. 54
A.10 Plot of the EEG signals marking bad segments. 55
A.11 Plot of the EEG signals after epoching. 56

B.1 Plot of the power spectrum data of raw EEG signals. 57
B.2 Plot of the power spectrum data after filtering the EEG. 58
B.3 Time frequency analysis on channels of interest. 59

C.1 Steps in the computation of the MI. 62

D.1 Linear mixed model menu. 63

List of Tables

5.1 p-values for the coefficient estimates in the first repeated-measure linear mixed-effect model (rmLMM). This considers the interaction between Group and Channel. 30
5.2 Average mean MI values across both runs. 31
5.3 p-values for the coefficient estimates in the second rmLMM. This considers the interaction between Group and Channel. 31
5.4 p-values for the coefficient estimates in the third rmLMM. This considers the interaction between Group and Channel. 32
5.5 Average mean z-score values across both runs. 33
5.6 p-values for the coefficient estimates in the fourth rmLMM. This considers the interaction between Group and Channel. 34

Acronyms

f_A	amplitude frequency *(pp. 11, 61)*
f_p	phase frequency *(pp. 11, 61)*
ALS	Amyotrophic Lateral Sclerosis *(pp. 1–4, 7–9, 13–17, 19, 21, 23, 25, 27, 29, 31–33, 35–38, 64)*
AUC	area under the curve *(pp. 31, 32, 36)*
CFC	cross frequency coupling *(pp. 10, 14, 61)*
DTI	Diffusion Tensor Imaging *(p. 9)*
E/I	excitation/inhibition *(pp. 7, 11, 14)*
ECG	electrocardiography *(pp. 8, 17, 18)*
EEG	electroencephalography *(pp. xv, xvi, 3, 4, 7, 8, 15, 17, 18, 20, 25, 37, 47–51, 55–58)*
EMG	electromyography *(pp. 2, 8)*
EOG	electrooculogram *(pp. 17, 18)*
fMRI	functional Magnetic Resonance Imaging *(pp. 7, 13, 14)*
ICA	independent component analysis *(pp. xvi, 20, 52–54)*
IQR	Interquartile Range *(p. 25)*
LFP	local field point *(p. 10)*
LMN	lower motor neurons *(pp. 1, 3)*
LSMeans	least square means *(pp. xv, 29–32, 34, 35)*
MEG	magnetoencephalography *(p. 7)*
MEP	motor evoked potential *(p. 13)*
MI	Modulation Index *(pp. xv–xvii, 11, 16, 22, 24, 25, 27, 29–32, 36, 37, 39, 61, 62)*

MRI Magnetic Resonance Imaging *(pp. 9, 13)*

PAC phase-amplitude coupling *(pp. xv, 3, 4, 10–12, 14–16, 21–23, 25, 27, 28, 31, 32, 34, 36–39)*

PT perceptual threshold *(pp. 18, 19, 24, 38)*

REM rapid eye movement *(p. 15)*

rmLMM repeated-measure linear mixed-effect model *(pp. xvii, 25, 27, 29–35)*

ROC receiver operating characteristic *(pp. xv, 25, 27, 31–33, 36)*

SEP somatosensory evoked potential *(pp. 8, 9, 17–19, 21, 28, 38)*

TMS Transcranial Magnetic Stimulation *(pp. 7, 13)*

UMN upper motor neurons *(pp. 1, 16)*

1

Introduction

1.1 Context and Motivation

Amyotrophic Lateral Sclerosis (ALS) is a heterogeneous neurodegenerative syndrome characterized by the degeneration of upper motor neurons (UMN) – neurons that extend from the cortex into the spinal cord and brain stem –, and lower motor neurons (LMN) – neurons that extend from the brain stem or spinal cord into the muscle [2], as shown in Figure 1.1. This degeneration leads mainly to motor symptoms, such as muscle weakness due to skeletal muscle atrophy, spasticity and dysphagia [2]. However, over the last 20 years it has been determined that extra-motor symptoms can occur in as many as 50% of ALS patients, for instance behavioural changes, and language difficulties that can eventually result in frontotemporal dementia [3, 4], proving ALS to be a multisystem disorder. With the progression of symptoms, respiratory paralysis commonly leads to death within two to five years [3].

For every 100,000 individuals, there are about three to five new instances of ALS each year, with the disease being more common in older adults, primarily affecting those in their middle to late 50s, as its incidence and prevalence rise with age [3]. The family history of 10% of ALS patients points to an autosomal dominant inheritance pattern – familial ALS (around 50% of these are due to *C9orf72* gene modifications) – while the remaining 90% are considered to have sporadic ALS and do not have any family members who are affected [4].

About two-thirds of patients develop spinal ALS and experience unilateral distal muscle weakness and atrophy in their upper or lower limb muscles, while the remaining one-third of patients show bulbar ALS and suffer with similar symptoms in their bulbar muscles[1]. Despite the existence of treatment options to manage many of the symptoms of ALS[2], to what concerns the treatment of the disease there are no drugs developed for the effect. The only "disease-modifying" drug approved in European countries so far is Riluzole which can extend mean patient survival by three to six months; plus, recent

[1] group of muscles in the head and neck

[2] such as spasticity, muscle cramps, emotional lability

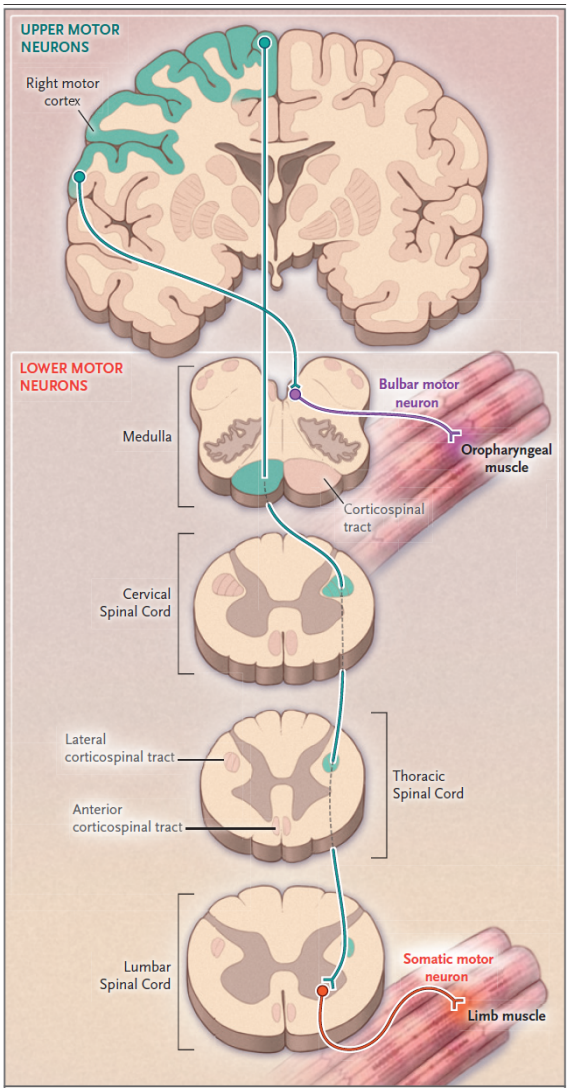


Figure 1.1: The Motor System. Reproduced with permission from [3], Copyright Massachusetts Medical Society.

studies show promising results with Edaravone [4]. Our incomplete understanding of the pathogenic pathways that cause ALS and how they impact the general integrity of brain networks is a major obstacle to develop effective treatments for the disease [2].

While there is no satisfactory treatment found up to now, also the diagnosis is rather imprecise and poorly defined, taking about 12 months to achieve. This, is primarily made by clinical examination, combined with electromyography (EMG) to establish the level of denervation, and followed by laboratory tests to exclude out reversible illnesses that may mimic ALS[3] [4].

Clinical evidence for degeneration at both the spinal and cortical levels is necessary for the diagnosis, yet cortical dysfunction-related symptoms are typically hidden by initial symptoms associated with spinal dysfunctions. According to the dying-back hypothesis,

[3] for example, peripheral neuropathy, Lyme disease, vitamin B12 deficiency, thyroid disease, and metal toxicity

ALS disease was thought to have its origins in the LMN and progress retrogradely from the neuromuscular junction into the central nervous system [5]. With this, it was originally believed that because ALS destroys the motor system, the disease exclusively affected motor neurons. Nonetheless, there is mounting proof that ALS also affects sensory neurons and comparable pathogenic alterations in sensory neurons have been reported in disease-modelling mice [6]. Nowadays, ALS is increasingly being recognized according to the dying-forward hypothesis, where it starts in the pyramidal neurons of the motor and pre-motor cortices and progresses through antegrade mechanisms to induce malfunction and death in the spinal and bulbar motor neurons [5].

Muscle spindles are innervated by proprioceptive peripheral nerve endings. These, directly send the changes detected in muscle length, velocity, and tension to α-motor neurons. Thus, ALS-related motor decline is likely affected by the degeneration of proprioceptive sensory neurons, specifically Ia/II proprioceptors. It has been demonstrated, long before motor symptoms manifest in ALS mice models, that some neuromuscular spindles present structural abnormalities and that Ia/II afferent fibres start to degenerate concurrently with the onset of the first peripheral motor denervation (neuromuscular junctions) [6]. This finding suggests that despite with slower kinetics, sensory fibres of spindle origin are equally prone to degeneration in ALS as motor fibres. It is quite likely that this sensory impairment disturbs the homeostasis of sensorimotor networks, which in turn leads to motor degeneration.

Along with that, a key characteristic of ALS has been shown to be cortical hyperexcitability, which occurs before neurodegeneration sets in and is correlated with biomarkers of motor neuron death [7, 8].

For the presented reasons, there is a crucial need for a biomarker of cortical dysfunctions in ALS for an easier diagnosis of the disease. Naturally, a question is raised on whether a new way of evaluating cortical dysfunctions at the level of sensorimotor network in ALS could be through electroencephalography (EEG) analysis given its low cost, high temporal resolution and easy implementation in both animal and human models. Currently, this procedure is poorly or not used whatsoever in ALS, even if it allows an evaluation of brain connectivity making it viable to identify biomarkers of cortical excitability.

1.2 Objectives

The main goal of this project is to propose a novel biomarker of cortical dysfunctions in ALS that can be extracted from EEG analysis in stimulated data, in particular through phase-amplitude coupling (PAC) between slow and fast oscillations.

Allied to the above mentioned goal, and part of the project in development, there are two other objectives. Those are:

- Adapt the existing pipeline to perform PAC analysis in stimulated data, through scripts developed in *Python*.

- Test whether PAC is altered in ALS patients after peripheral nerve stimulation.

The hypothesis is that PAC analysis of stimulated EEG would give rise to a more reliable evaluation of PAC and provide a fresh perspective on the neural connectivity and its alterations in ALS. This could offer a more trustworthy marker of cortical dysfunctions if a relationship between the brain cortical excitability and PAC in humans, especially ALS patients, was found and understood.

The clinical importance of this goal lies in the possibility of unveiling a new way to help with the diagnosis of ALS, enabling a quicker and more precise identification of the condition. Also, it brings the opportunity of clarifying the neuropharmacology in preclinical models and the cellular mechanisms underlying PAC alterations, which will open up novel therapeutic prospects [9].

1.3 Thesis outline

Apart from this initial introductory chapter, the current thesis is structured into an additional five chapters, which main contents are presented below.

Chapter 2, entitled "Concepts", introduces key theoretical concepts necessary for understanding the contents of this work.

Chapter 3, entitled "State of the Art", begins by looking at some techniques that have already been used to investigate cortical hyperexcitability in the brain. It then delves into PAC and its role in cortical excitability. Finally, it unveils its association with neurodegenerative disorders, particularly considering recent results showing deficiencies in ALS, and paving the path for conducting this endeavour.

Chapter 4, entitled "Methods", details the methodologies employed in the study, as well as to describe the used data. It begins by detailing the dataset used, the process of recording and preparing EEG data, and the methods applied for signal analysis, highlighting both obstacles encountered and solutions developed. The chapter finishes with a statistical analysis of the findings, emphasising the need for rigorous methodological approaches in neurophysiological research.

Chapter 5, entitled "Results and Discussion", presents the main findings of the employed methods mentioned in the preceding chapter, alongside their discussion.

Chapter 6, entitled "Conclusions", lays out the key topics that were discussed and the outcomes that were attained. In addition to exploring potential future directions, it offers a summary of the primary constraints of this project.

Declaration of Originality

The research work described in this dissertation was carried out in accordance with the norms established in the ethics code of Universidade Nova de Lisboa. The work described and the material presented in this dissertation, with the exceptions clearly indicated, constitute original work carried out by the author.

2

Concepts

2.1 Excitation/Inhibition Balance

Excitation signifies increased neural activity, where neurons are more likely to generate signals and communicate with each other, and is akin to pressing the accelerator in a car. On the other hand, inhibition acts as the brakes, reducing the overall activity of neurons and aiding with sinchrony of neural networks.

In the brain, excitatory and inhibitory inputs onto major neurons must be coregulated in order to maintain a balance between activity and stability. Changes in the excitation/inhibition (E/I) balance lead to changes in excitability and a reduced ability to receive incoming information. The excitability of local circuits is altered in many neurodevelopmental and neuropsychiatric illnesses, indicating changes in synaptic excitation, inhibition or both, that may play a role in their pathogenesis [10].

Excitotoxicity is an intricate process initiated by the activation of glutamate receptors, leading to dendritic degeneration and neuronal injury or death [11]. An excessive buildup of glutamate has the potential to induce neuronal excitability [12], a process mitigated by Riluzole, an anti-glutamatergic agent. This suggests that motor neuron excitotoxicity could play a detrimental role in the progression of ALS [13]. Moreover, Edaravone, functioning as an antioxidant, exhibits promising outcomes by alleviating the oxidative stress responsible for neuronal death in individuals diagnosed with ALS [14].

2.2 Cortical Hyperexcitability

The term "hyperexcitability" describes a shift in neuron excitability that makes neurons more prone to firing action potentials in response to external stimuli, reflecting therefore a cortical dysfunction [13]. Clinically, it appears as hyper-reflexia, spasticity, and profuse fasciculations [15].

Several methods, including threshold tracking paired-pulse Transcranial Magnetic Stimulation (TMS), EEG, magnetoencephalography (MEG), and functional Magnetic Resonance Imaging (fMRI), can be used to therapeutically evaluate cortical excitability.

When combined, clinical data from gene sequencing, neuroimaging, and electrophysiology have shown that ALS patients exhibit cortical hyperexcitability even before they exhibit symptoms, which establishes it as an initial feature of ALS [13].

Besides, considering that the only Food and Drug Administration (FDA)-approved drugs - Riluzole and Edaravone - demonstrating efficacy in treating ALS are associated with cortical hyperexcitability, it becomes imperative to delve into a comprehensive study of this phenomenon [13].

Furthermore, it has been shown that in later stages of ALS, cortical hyperexcitability is more noticeable, meaning it evolves as the illness progressed [16].

2.3 Electroencephalography

EEG captures the brain's spontaneous electrical activity over a brief period of time, presenting this measure in voltage (volt, V). Renowned for its utility in investigating neurocognitive processes, this tool offers a high temporal resolution, directly capturing the delicate variations of neural activity [17].

The 10/20 international system is a standardized method for electrode placement on the scalp in order to acquire the EEG signal. Electrodes are positioned at specific locations based on the distances between anatomical landmarks. The "10" and "20" refer to the fact that the distances between adjacent electrodes are either 10% or 20% of the total front-back or right-left distance on the scalp. This system ensures consistency in electrode placement across individuals, facilitating accurate comparison of EEG data for studying brain activity and neurocognitive processes.

2.4 Somatosensory Evoked Potentials

An evoked potential is produced when a compound action potential is generated beyond the resting threshold of sensory receptors or afferent nerve bundles. The electrical activity response recorded at the skin's surface after carefully regulated sensory or peripheral nerve stimulation is known as somatosensory evoked potential (SEP). Therefore, SEPs are time-locked to a stimulus via a pretrigger rather than continually recorded to spontaneous stimuli like EEG [18]. Traditionally, SEPs peak amplitudes fall below 10 μV, which is less than EEG (tens of μV), EMG (mV), and electrocardiography (ECG) (V).

For characterizing SEP waveforms, a letter denoting its peak's polarity (positive or negative) is allocated. Thus, according to convention, a downhill deflection is assigned a positive (P) polarity, while an upward wave deflection is assigned a negative (N) polarity. Additionally, an integer is assigned depending on the post stimulus latency (in ms) at which they appear in a healthy population. This description is exemplified in Figure 2.1.

Changes in brain activity can be deduced from these peaks' amplitude (μV) and delay. SEPs can be used as a neurophysiological technique to assess how the central nervous

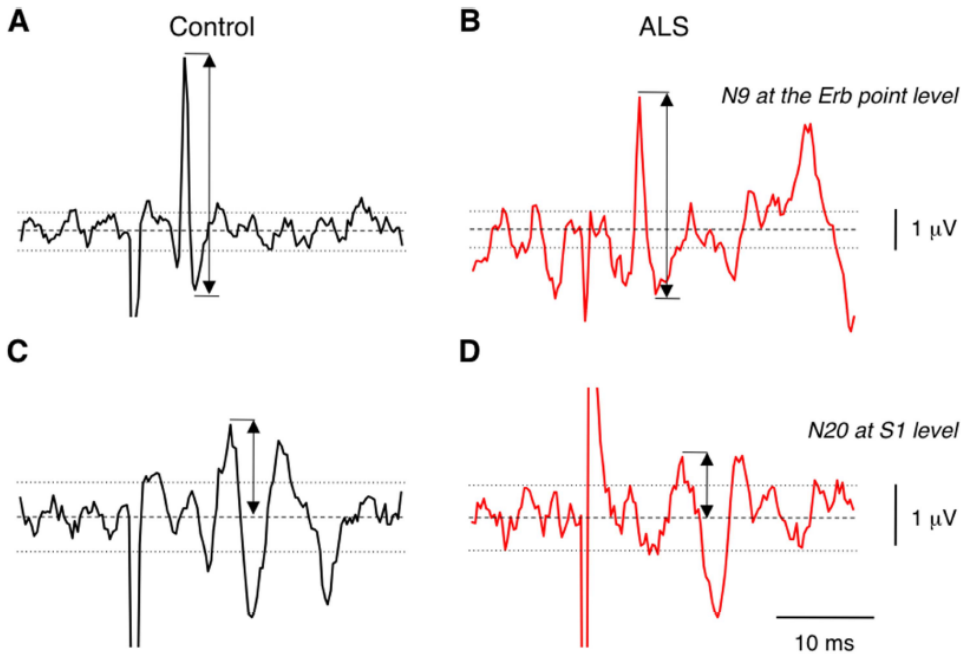


Figure 2.1: N9 and N20 amplitude. Raw signal (in μV) from recordings at the Erb point level (A and B) and at cortical level (in front of S1, C and D). Reproduced with permission from [19].

system reacts to alterations in its surroundings, i.e., reflect the neuroplasticity related to a perceptual or motor task. In cases of pathology where its origin is, for instance, degenerative, peaks may occur either later or not at all [18]. SEPs have been employed to evaluate the presence of elevated somatosensory excitability, i.e., the hyperexcitability of the sensory cortex [20].

Studies have shown that, in early stages of the disease, up to 60% of ALS patients presented SEPs abnormalities when compared to control groups [19, 21]. In addition, it has been shown, using diffusion Magnetic Resonance Imaging (MRI), that white matter in the posterior spinal cord is altered at an early stage of the disease. By combining Diffusion Tensor Imaging (DTI) and SEP, up to 85% of the patients demonstrated a sensory impairment, despite the fact that they did not have any clinically proven sensory disorders [19].

2.5 Neuronal oscillations

Biological systems in general, and particularly the electrical activity in the brain are rife with oscillatory activity [22]. Thus, one way to think of neural oscillations is as rhythmic variations in cortical excitability, representing the coordinated activity of neural groups. Detected oscillations may exhibit variations in their frequency in Hertz (Hz), featuring

distinct bands such as delta (1-4 Hz), theta (4-8 Hz), alpha (8-12 Hz), beta (12-30 Hz), and gamma (above 30 Hz).

The way that a stimulus is processed by neurons varies according to its timing in relation to the oscillation phase that is currently occurring. Stimuli time-locked to the local field point (LFP)[1] trough may be processed more quickly or thoroughly than stimuli time-locked to the oscillatory waveform's peak if high neuronal excitability is linked to the oscillation's trough [23].

2.6 Phase-Amplitude Coupling

The relative timing (phase) and power (amplitude) of rhythmic activity in individual neurons, networks, and systems are interdependent, as shown by neural oscillations. Nested, multiplexed signals are the result of simultaneous interactions between various neural activity frequencies, and this cross frequency coupling (CFC) might represent a significant portion of the synchronised neural activity thought to be responsible for brain functioning [22].

The statistical relationship between a low-frequency brain rhythm's phase and the high-frequency component of electrical brain activity's amplitude, is known as PAC. While high-frequency power rises represent either a general increase in population synaptic activity (broad-band power increase) or selective activation of a connected neuronal subnetwork (narrow-band power increase), low-frequency phase reflects local neuronal excitability and is linked to behaviourally significant events. Additionally, PAC offers a useful way to combine activity over several temporal and spatial scales [23].

Research shows that as the size of a neural assembly in the brain increases, the synchronization frequency of its activity decreases, indicating that longer-range interactions are mediated by lower frequencies [24]. In PAC, the phase of low-frequency rhythms modulates the amplitude of high-frequency oscillations, as shown in Figure 2.2 [25].

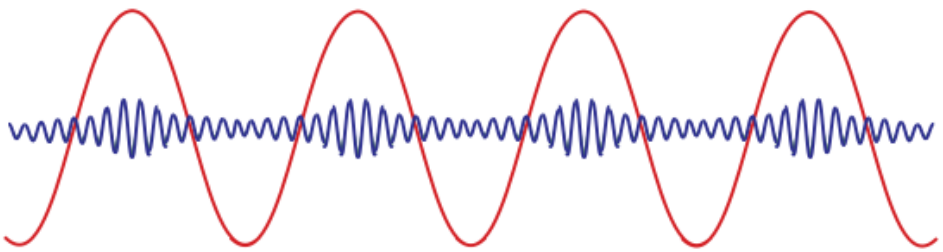


Figure 2.2: PAC - Gamma amplitude modulated by theta phase. Reproduced with permission from [9].

[1] measures of synchronized population activity

The knowledge of brain function and dysfunction in various clinical situations may be aided by changes in the E/I balance, which can impact neural oscillations, including PAC patterns.

Interestingly, studies have not only shown that PAC strength can change rapidly within hundreds of milliseconds from no coupling to significant PAC and back, but it also demonstrated that distinct brain areas exhibit distinct coupling patterns and temporal modulation. The results imply that PAC is partially or entirely related to continuous active cognitive demands. Thus, this lends credence to the idea that PAC serves a functional purpose [26].

2.7 Modulation Index

The Modulation Index (MI) is what measures the intensity of coupling, besides detecting its existence. The two frequency ranges of interest are the "phase-modulating" and "amplitude-modulated" and are commonly referred to as phase frequency (f_p) and amplitude frequency (f_A). It should be highlighted that the MI loses time information, therefore it is unable to determine if coupling happened continuously throughout the epoch under study or only in spurts. In contrast, metrics based on the regression or coherence between the envelope amplitude of f_A and f_p can help us determine how consistent the coupling was throughout the course of the entire era [25].

Limited-time datasets have been analysed to investigate PAC for subsequent event epochs during maze runs. By using this measure on several frequency band pairings consisting of f_p and f_A bands stepped across task time, phase-to-amplitude comodulograms can be created [26].

The higher the value of the MI, the stronger the phase-to-amplitude modulation, since if no coupling exists between the pair of frequencies, then the amplitude distribution over the phase bins is uniform, i.e., for each phase of the f_p oscillation, the amplitude of f_A remains constant [25].

2.8 Comodulogram

The MI can be utilised to create a phase-to-amplitude comodulogram graphic, a bi-dimension frequency map that reports the degree of coupling between several bands at once. This pseudocolor graphic shows the degree of connection between multiple pairs of narrowed-filtered frequency bands and is used to discuss results [25, 26]. The MI value is represented in a comodulogram as demonstrated in Figure 2.3 [25].

By scanning frequency band pairs and applying the PAC measure to each one, the comodulogram is produced. When no presumptions regarding the phase-modulating and amplitude-modulated frequency bands are made, this approach is appropriate for looking for PAC [25].

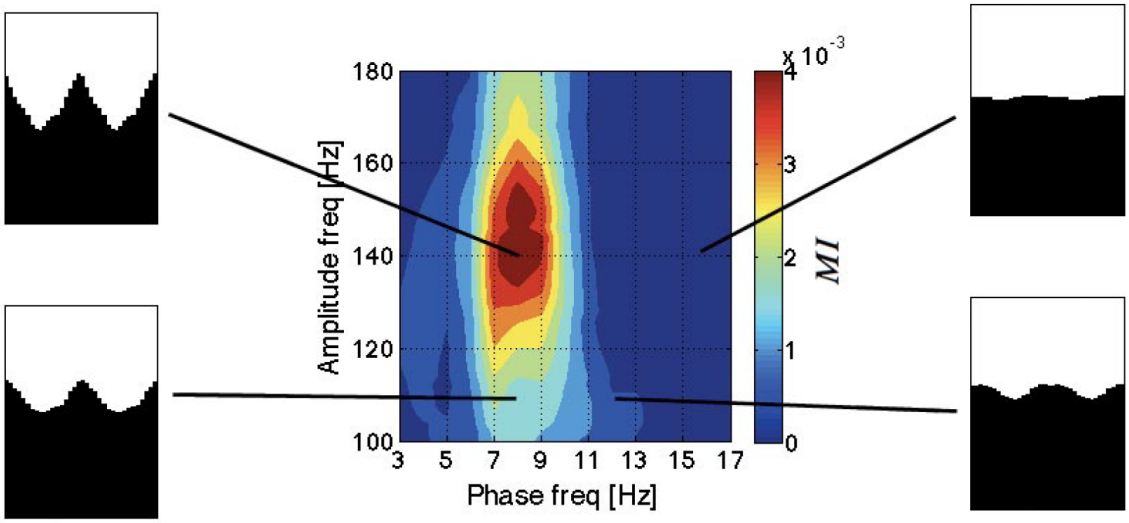


Figure 2.3: Comodulogram: example of PAC intensity. Reproduced with permission from [26], Copyright (2008) National Academy of Sciences.

3

State of the Art

3.1 Cortical excitability in ALS

3.1.1 Transcranial Magnetic Stimulation

One technique that has been mainly used to search for cortical dysfunctions' biomarkers is TMS which has been studied for an ALS diagnosis since it provides a non-invasive and painless evaluation of cortical function. This was shown to be a reliable procedure, distinguishing ALS from other mimicking disorders and hurrying the diagnosis in about eight months [27]. While TMS is a technique that stimulates brain nerve cells with magnetic fields, suprathreshold TMS pulses are used to activate the primary motor cortex, which causes a motor response in the targeted muscle. This reaction is referred to as the motor evoked potential (MEP). Recently, the threshold tracking strategy that tracks the stimulus intensity for a target amplitude has been implemented [28].

Overall, threshold tracking TMS studies show that motor cortex hyperexcitability is a characteristic of ALS that frequently occurs before the symptomatic phase [13].

Still, some studies have not found any significant longitudinal changes in TMS parameters over time [29], contradicting other suggestions that TMS may have a clinical utility in assessing the disease development [30]. These findings argue against the usefulness of TMS in tracking the progression of ALS disease as it can be difficult to implement with the progression of the disease due to muscle atrophy and weakness or possible limitations in cortical excitability. Moreover, it remains a specialised technique that requires a certain technology and level of training [31], and given the possibility of variability in between subjects, careful consideration should be given to the method's standardisation [13].

3.1.2 Functional Magnetic Resonance Imaging

Amongst some of the neuroimaging techniques used to evaluate cortical dysfunctions in ALS, fMRI is the most utilized to assess the disease. Due to its ability to rule out pathology, MRI is an essential component of the diagnostic procedure for ALS [32].

Because resting-state fMRI displays the convergence of structural and functional information, it presents a unique opportunity to study ALS as a "system degeneration" through its visualisation of interconnected cerebral networks [32].

Yet, some limitations with fMRI exist such as the degree of incapacity of the patient which can immediately affect his or her capacity to complete the assigned work, analysis of patients with a relatively long disease duration leading to an overestimation of effects, and the high costs and complex implementation of the exam [18, 33].

3.2 Phase-Amplitude Coupling

3.2.1 PAC dependence on cortical excitability

It is well known that there is PAC between gamma oscillations and other slower rhythms in both the same and separate brain areas [34].

Some papers point to a potential connection between PAC and E/I balance [34, 35], specifically that local high-frequency oscillations can be triggered and grouped by the slow oscillations, and that these CFCs may indicate global cortical excitability. Despite the lack of concrete evidence from experiments, a study revealed promising results on a new way to predict seizures through a brain excitability measure that is determined by the coupling between high-frequency amplitude and low-frequency phase [36].

Additionally, fast-firing basket cells have been proposed as a potential critical component of CFC. This makes sense because slower oscillations frequently lure several other types of interneurons, which in turn inhibit basket cells, and short-lived gamma oscillations result from these coordinated activities of inhibition and excitation [34]. Thus, one efficient method for functionally connecting active cortical circuits is PAC.

3.2.2 PAC alterations in neurodegenerative diseases

There is curiosity in the potential involvement of abnormal CFC in neurologic illnesses due to its varied roles in cortical function. For instance, atypical beta- and gamma- band activity synchronisation has been linked to schizophrenia [37]. Further, in the case of Parkinson Disease excessive cortical PAC was found [37, 38], but also in Alzheimer's disease [39–42], and frontotemporal dementia [43], PAC was shown to be compromised. These findings urge that alterations in PAC could also occur in other neurodegenerative diseases such as ALS.

3.2.3 PAC limitations and assessment

While the standard CFC analysis and its physiological interpretation holds great potential for understanding both healthy and pathological brain function, certain challenges arise. Current CFC measures of PAC lack specificity, making it problematic to

automatically conclude, as often done in the literature, that the phase of a low-frequency oscillation modulates the power of high-frequency activity. One of these problems lies with the choice of the phase and amplitude bandwidth sizes: the first needs to present a meaningful phase, whilst the second needs to include the side peaks produced by the lower frequency. Using the right approaches to minimise phase and amplitude dynamics distortion and lower the amount of false positives is another issue [44].

Hence, the main challenge is to determine if the emerging phase-amplitude correlation between two bands is the result of a signature of interactions between rhythms or a common drive that is produced by either internal or external input.

To help with this problem, a series of recommendations and stricter procedures for PAC analysis has been developed [44].

One common way to assess PAC is through *pactools* package, in *Python*, which allows to estimate the coupling in neural time series [45].

Nevertheless, in the laboratory where this project was conducted, a pipeline for PAC analysis in MNE-*Python* has been developed to study PAC in resting-state EEG signals, and it is suggested that all of the above listed concerns be addressed and taken into consideration, allowing a broader application of the method [46].

3.2.4 PAC preliminary results in ALS

It has been shown that in mice, PAC revealed deficits in ALS even before symptom onset. Additionally, from the presymptomatic stages to the end stage of the disease, there was impaired theta-gamma PAC during both rapid eye movement (REM) sleep and active wakefulness, indicating persistent cortical dysfunction [9].

In humans, and with a resting state duration of five minutes, PAC between theta and gamma rhythms was studied on five central channels as shown in Figure 3.1.

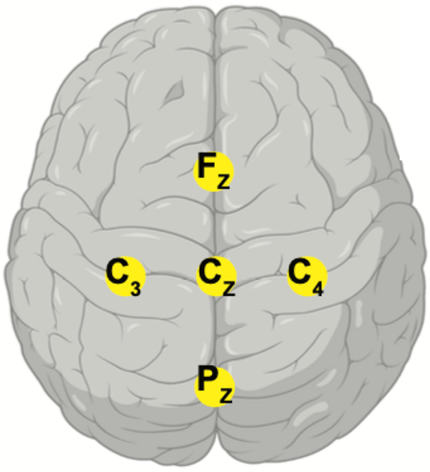


Figure 3.1: Five central electrodes placed in the scalp. Reproduced with permission from [9].

From this study, preliminary main results reveal that theta-gamma PAC is significantly depressed in ALS patients, particularly in C3 channel which is associated with the primary sensorimotor area in the dominant hemisphere, reflecting cortical hyperexcitability. The MI diminished with disease progression, being smaller in fast progressors as opposed to slow progressors [9], and revealing that PAC deficits in ALS correlate with the continuous loss of motor functions as opposed to UMN impairment, demonstrating its potential to detect cortical dysfunction regardless of UMN injury.

Moreover, results under review indicate that the strength of the findings in resting condition is significant, uncovering a very high discriminative ability and supporting the theory that the results in stimulated data could be even stronger since the brain responds in a "constant" way, allowing it to determine which area is active and why.

4

Methods

All computing referenced in this and further Chapters was conducted using *Python* coding language and *Spyder* editing software.

The analyses were carried out using MNE-*python* [47], an open source library for processing, analysing and visualising human neurophysiological data, such as EEG data, and necessary supplementary packages for the making of custom scripts were used. Plotting of results was done using *Python* or JMP® software.

4.1 Data acquisition

The data used is part of SOMALS2 protocol that has been authorised by the national ethical authorities (CPP Ouest II Angers, n.°18.07.11.57804-2018/58; RCB 2018-A00789-52), and the National Institute of Health and Medical Research INSERM ethics committee (protocol #C17-70). The dataset had been previously acquired and is composed of 26 healthy controls (age avg. 63.42 ± 2.08 years) plus 26 sporadic ALS patients (age avg. 60.44 ± 2.47 years), all under riluzole, that were studied at an early-stage post-diagnosis. Both groups are age and sex matched with one-third of them being females and two-thirds being males, and prior to inclusion, each participant gave written, informed consent.

EEG recordings (4 kHz sampling rate, bandpass 0.03-1330 Hz) were obtained on the Elekta Neuromag® TRIUX (Stockholm, Sweden) at the Centre of NeuroImaging Research (CENIR) of the Brain Institute (ICM, Pitié-Salpêtrière Hospital, Paris, France). An EEG cap with 74-Ag/AgCl electrodes was placed following the international 10/20 system (EasyCap GmbH, Herrsching, Germany), and positioned such that the Cz electrode was above the anatomical vertex, as illustrated by Figure 4.1. At the same time, non-neural signals such as the ECG, electrooculogram (EOG), and stimulation (SEP) electrodes were recorded.

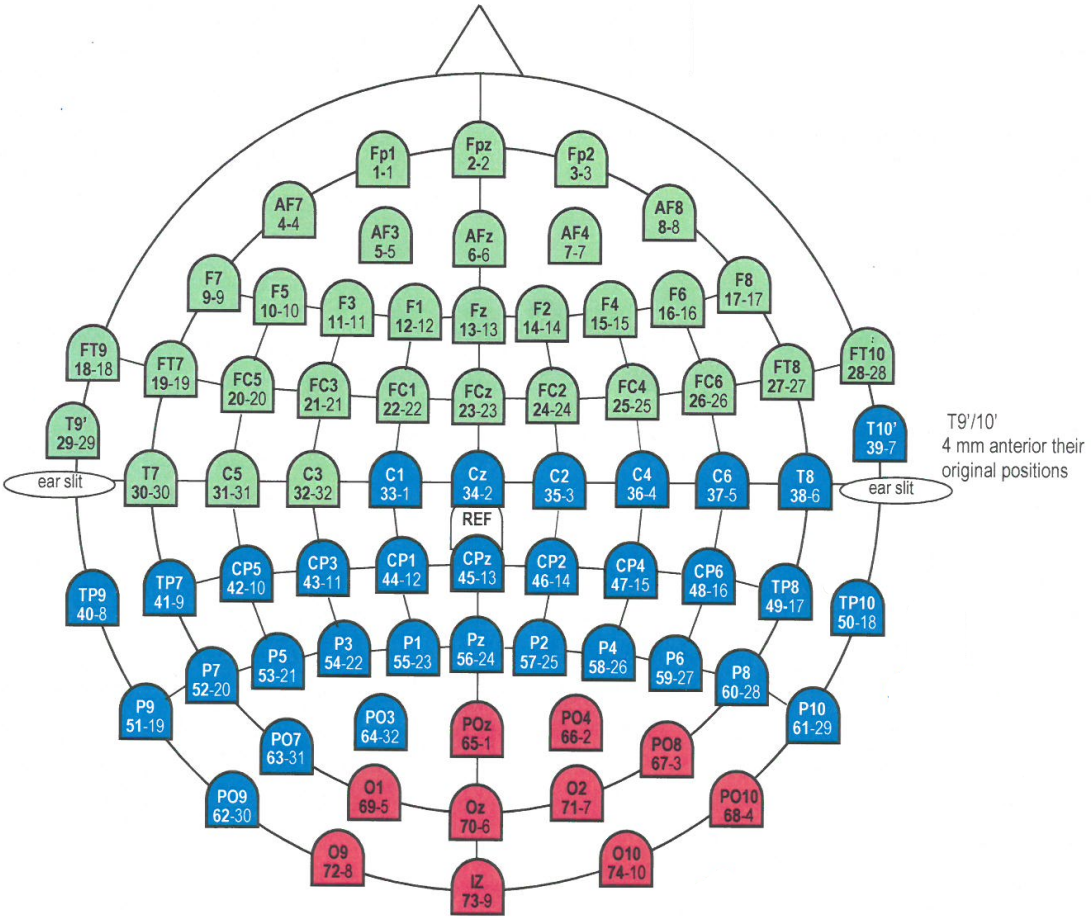


Figure 4.1: 74 channels EEG brain cap (EasyCap GmbH).

4.2 Experimental protocol

1. **Equipment placement -** The electrode cap is placed on the head, and the electrodes of interest are prepared to collect the signal. Over the EEG cap, gel is spread. Two electrodes adhered to the right eye along the vertical axis to collect the EOG; two electrodes in the horizontal plane on both temples to collect the EOG; two electrodes around the chest to collect the ECG; two electrodes at the Erb points to collect the SEP; and a ground electrode on the left shoulder blade are all set into place.

2. **Stimulation software initialisation -** The stimulator (DS7A, Digitimer Ltd, Hertfordshire, United Kingdom) is started and connected to Neuromag® TRIUX. Each stimulation is delivered using two surface silver electrodes placed at the wrist, and once the software is initialised, it is prepared to deliver stimuli at a frequency of 1.79 Hz, with intensities ranging from 1.5 to 9 times the perceptual threshold (PT) (1.5, 3, 6 and 9x the PT).

3. **Signal acquisition -** Recordings start, and the ulnar nerve is stimulated at the wrist level (N = 300 stimuli with a square pulse of 1 ms). Each recording captures one stimulation intensity, and with two runs per intensity, there will be a total of eight recordings per subject.

4. **Acquisition conclusion -** The softwares are shut down, and the equipment is removed.

Given that the average duration of the cortical SEP is less than 500 ms, and the stimulation frequency was 1.79 Hz, the average inter-stimulus interval (ISI) for the stimuli applied was 555.8 ms. The stimulation montage was placed at the wrist over the ulnar nerve to stimulate peripheral sensory fibers from the subject's dominant hand, as seen in Figure 4.2. For controls, dominant hand was stimulated, whereas in patients only if the latter had no muscle weakness on their dominant hand. During recordings, the subject was instructed to not count the stimuli and to fix their gaze on a cross in front of them.

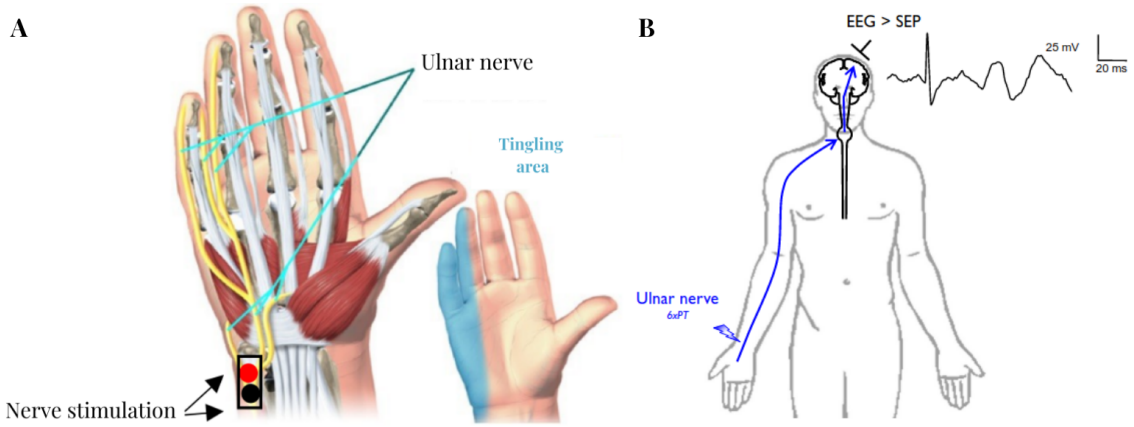


Figure 4.2: Representation of the stimulation applied in each subject. (**A**) - Electrodes placement for the experiment. (**B**) - Illustration of the stimulus response until the brain.

The ulnar nerve was chosen to apply stimulation because it is the nerve which controls most of hand muscles, one the main first site of ALS disease. Besides, research suggests that SEPs from the ulnar nerve tended to be more altered in ALS when either the median or ulnar nerve was stimulated [48].

Moreover, it makes sense to stimulate the wrist area since, by doing so, it activates the area of the brain that is associated with movement and cortical function - the sensorimotor area - [20, 49, 50], where the symptoms of cortical dysfunction are present, but are typically masked by the initial symptoms of spinal dysfunction. From the applied intensities, 6x PT produced a strong perception, associated with a firm motor response in the thumb. This intensity was selected to pursue the desired analysis since it has been demonstrated to be the one at which evoked responses are stronger [49].

4.3 EEG preprocessing

To clean the acquired data, ie, to preprocess it, a pipeline was developed that is constituted of the following steps, illustrated by Figure 4.3. An example of each step of the pipeline can be found in Appendix A.

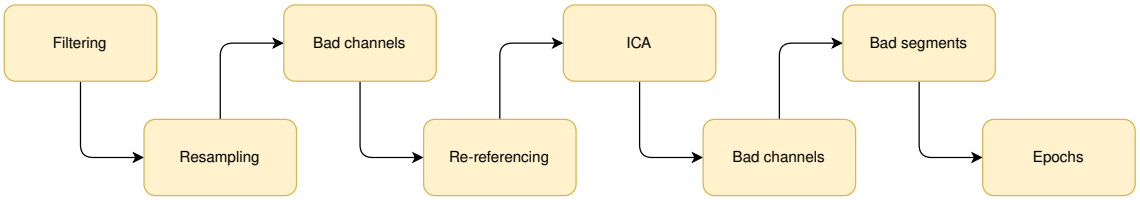


Figure 4.3: Schematic containing the steps followed in the preprocessing pipeline.

The previously collected data was first parsed and filtered: a notch filter for power line harmonics at 50, 100 and 150 Hz (*raw.notch_filter* function), followed by a bandpass filter (*raw.filter* function) between 0.1 and 500 Hz. In order to preserve any physiological response of relevance, these frequencies were selected following a thorough examination of the data power spectrum (*raw.compute_psd* function) for the notch and a time-frequency analysis for the bandpass filter. The conducted analyses can be seen in Appendix B.

The data was then resampled to 1000 Hz, reducing memory usage. Afterwards, there is a round of bad channels which aims to identify any bad channel that may exist within the 74 recorded. The *pyprep.NoisyChannels* class provides a first detection of bad channels (using *find_all_bads* function), but a visual confirmation is needed to decide whether the selected channels should be kept, interpolated (*raw.interpolate_bads*) or definitely eliminated (*raw.drop_channels*). Following this step, an average re-referencing is made through *mne.set_eeg_reference* function, mainly to improve the overall quality of the signal by allowing a better comparison across electrodes.

After that, there is an independent component analysis (ICA) artefact detection stage which aims to separate and remove artefacts, such as eye blinks or saccades, heart beats, and muscle movements from the neural signals of interest. This happens by means of *mne.preprocessing.ICA* class, and once again, a visual inspection is needed to correctly identify which components to eliminate. Next, a new round of bad channels takes place, adhering to the previous premise, and immediately following, to preserve the integrity of the signal, it is imperative that bad segments be manually marked before moving on to the last stage.

Finally, the EEG time series is epoched in 500 ms windows, ie, the signal is divided into 500 ms intervals of time: 200 ms before, and 300 ms after the stimulus, by taking advantage of the stimulation channel STIM. With 300 applied stimuli, every recording will correspond to 300 epochs, some of which may be removed upon close inspection to produce final data that is suitable for analysis at a later time. The cleaned response of the brain around the applied stimuli can be observed in Figure 4.4 by averaging the epochs that resulted.

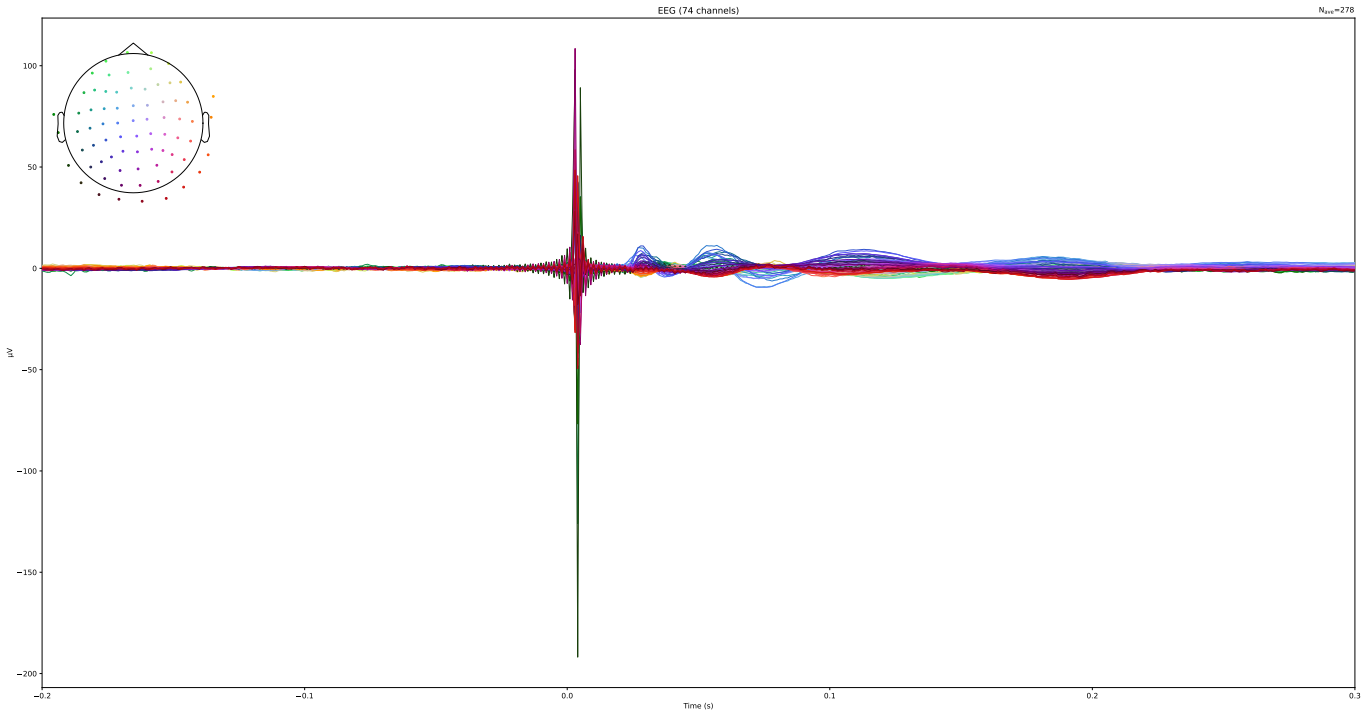


Figure 4.4: Plot of a brain average response, after preprocessing. Each colour represents a different channel as displayed on top left corner.

The work carried out to investigate the signal topography was developed during these epochs, and on specific windows within those, corresponding to early and late components of SEP. The post-stimulus period was the primary focus of this effort, corresponding to the window spanning 18 ms to 120 ms. This time frame agrees with the literature [48], as well as what can be seen by examining the data when averaging the two runs for each subject.

While no correlation between SEPs' early and late components has been found, it was shown that patients with ALS had higher depression in their late SEPs than in their earlier components [48, 51]. Further, recent results reveal a significantly more complicated cortico-cortical sensory network and substantially greater cortical activity during late components than just the importance of secondary somatosensory cortex that is acknowledged up to date [49].

4.4 PAC analysis

Given the existent preliminary results of PAC analysis in ALS resting-state patients, mentioned in Chapter 3.2.4, the rational next step was to investigate PAC in stimulated data, since this allows to study the brain's response to a direct activation of the sensorimotor area, as opposed to merely the brain's regular oscillatory activity.

In order to accomplish this, two approaches were tried: an initial one to adapt the existing pipeline for PAC analysis, and a second approach through *pactools*.

4.4.1 Adaptation of the existing pipeline

A first attempt was made to adapt the existing pipeline [46] to extract PAC in resting-state, based on Tort's method to calculate the MI [26]. The steps to calculate the MI accordingly to Tort can be seen in Appendix C. Yet, derived from this, two problems arose.

Originally, a low-frequency peak detection stage takes place in the pipeline in order to pursue PAC analysis. However, in the present case of study, despite having an epoch duration of 500 ms, the region of interest lasts much shorter, only about 100 ms. In a narrower time window, low frequency oscillations are less likely to be fully captured because their longer periods are longer than the window's allotted duration. As a result, this time span exhibits fewer, if any, distinct peaks in lower frequency bands (namely theta and alpha), leading to a limited number of epochs that meet the criteria to be studied.

Secondly, after extracting the phase of the low frequency and the amplitudes of the high frequency signal, and calculating PAC by extracting the MI, results are presented in the form of comodulograms. Understandably, these findings were compared with a "baseline" to provide significance to the results obtained – and for that it was created surrogate data.

4.4.2 Surrogate data problematic

Surrogate data is a technique used in time series analysis to test the null hypothesis that the original dataset could have been generated by a random process with the same statistical properties. This technique allows us to determine whether observed patterns in a dataset are due to intrinsic properties or random fluctuations. It is produced by randomly rearranging or modifying the original data while preserving certain characteristics, enabling a statistical measurement comparison between the original and surrogate data. In the case of PAC, this is usually accomplished by reorganising the amplitude's component part while keeping the phase. Significant differences suggest that the original data includes real structure or patterns, such as PAC in brain rhythms.

However, the ideal method for producing surrogate data remains elusive, especially when examining event-related potentials within a narrow analytical frame. Methods like circular shifting [46] or randomised trial shuffling [44] were attempted to implement for being the most reliable techniques.

- **Circular shifting:** in the first technique, the amplitude envelope is circularly shifted at a random position while keeping the phase intact.

- **Randomised trial shuffling:** the second strategy involves maintaining the phase for each epoch while shuffling the intact amplitude components between distinct epochs.

To verify the feasibility to use these two methodologies to produce surrogate data, a correlation study on the high frequency amplitudes' envelope was performed in between epochs as well as an autocorrelation within epochs themselves.

4.4.3 *pactools* approach

In light of the constraints mentioned above, some alterations were made to the initial approach, mainly abandon the attempt to adapt the existing pipeline and take advantage of *pactools*. This allowed to focus on a whole range of low frequencies as opposed to just the area around its peaks; and discard the use of surrogate data.

Firstly, to maintain a more uniform frequency band of investigation across all epochs rather than analysing different frequencies in each suitable epoch, it was determined to assess and analyse the entire frequency range of interest, in particular, to study the slightly higher frequency beta band. Not only to ensure the presence of activity, due the small window of analysis, but also because beta band is associated with the sensorimotor area in the brain and it has been shown to be intensified after stimulation [52–54].

Taking into account these new considerations, the aim was to study PAC between the low frequency beta band, from 12 to 30 Hz, and high frequency gamma band, from 30 to 100 Hz. Once the period and the bands of analysis were chosen, the *pactools* package was utilised to estimate beta-gamma PAC in the neural time series, using Tort's method [25]. The comodulograms between beta phase and gamma amplitude were constructed by subdividing each band into 30 (steps of 0.6 Hz and 2.4 Hz for beta and gamma, respectively). From these calculations, it was possible to extract the comodulogram's values - for the analysis in question, the mean and the max value for every desired channel and subject were taken.

The primary focus of the analysis was on the sensorimotor cortex, which is initially impacted in ALS, and its surrounds, as shown in Figure 4.5. This happens because the chosen electrodes cover the area of the brain known to be activated after receiving the stimulus [49]. Nevertheless, since the stimulation happens on one side of the body, only channels of interest in the associated controlateral hemisphere are significant. Thus, for someone who is aroused on the right side, the goal is to investigate the channels of interest in the left hemisphere, and vice versa.

4.5 Statistical analysis

To statistically assess and interpret the measures acquired after PAC calculations it is necessary to perform a statistical group analysis, in this particular case through the predictive analytics JMP pro® 17 software (SAS Inc., Cary, NC, USA).

The dataset used for analysis included observations of two runs and eight channels for each subject, comprising 25 ALS patients and 24 healthy controls. This number differs from the original number of subjects in the dataset (26 ALS vs 26 healthy) since 3 subjects were

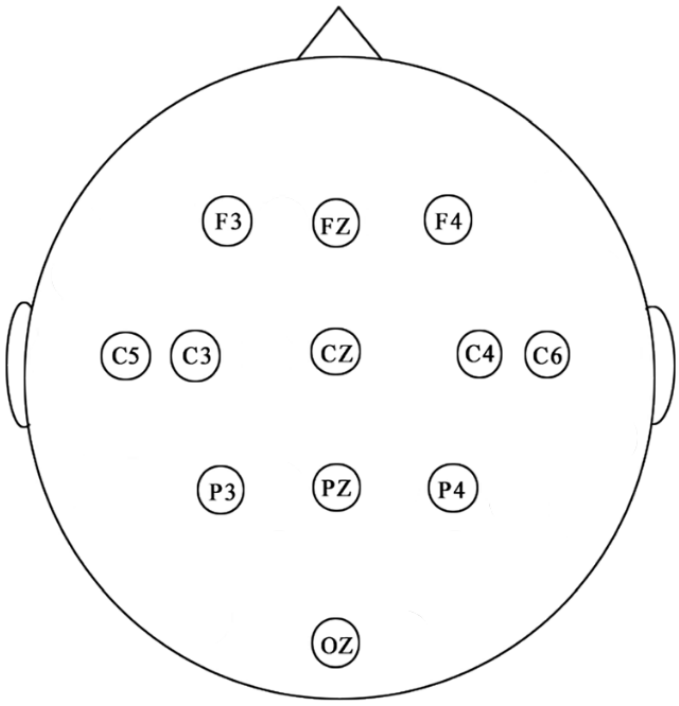


Figure 4.5: Scalp layout with channels of interest for the analysis.

not able to receive a 6x PT stimulation due to acquisition problems or lack of sensitivity, and were, therefore, disregarded from the present analysis.

It is important to take into consideration that the data extracted from the comodulograms originates from several channels of interest, depending on the stimulated side of the subject. Yet, the goal lies in studying the main channels from the controlateral hemisphere, irrespective of their left or right origin. Hence, channels must be renamed prior to conducting the analysis that will be explored in the next chapter:

- **F3 and F4:** F, representing the frontal channel to be studied.
- **C3 and C4:** Ci, representing the more inner central channel to be studied.
- **C5 and C6:** Ce, representing the more external central channel to be studied.
- **P3 and P4:** P, representing the parietal channel to be studied.
- **Fz, Cz, Pz and Oz:** were kept the same as they are situated in the interhemispheric sulcus and do not differ between subjects with different stimulation sides.

Analysis were performed on values retrieved from the post-stimulus period comodulograms: either the mean MI directly, or the mean z-score. A z-score was calculated for each point of the comodulogram according to the following equation:

$$z\text{-}score = \frac{x_{\text{post}} - \mu_{\text{pre}}}{\sigma_{\text{pre}}}, \tag{4.1}$$

where x_{post} represents each MI on the post-stimulus comodulogram, and μ_{pre} and σ_{pre} represent the mean MI and the standard deviation of the pre-stimulus comodulogram, respectively.

Z-score was chosen to compare the pre- with the post-stimulus condition as it is a common way to normalize data to limit the influence of recording conditions and reduce inter individual variability.

Upon confirmation that both data distributions are not normal, as seen in Figure 4.6, and prior applying the model, the dataset was investigated for outliers, according to the Interquartile Range (IQR) method, and the outliers found were removed.

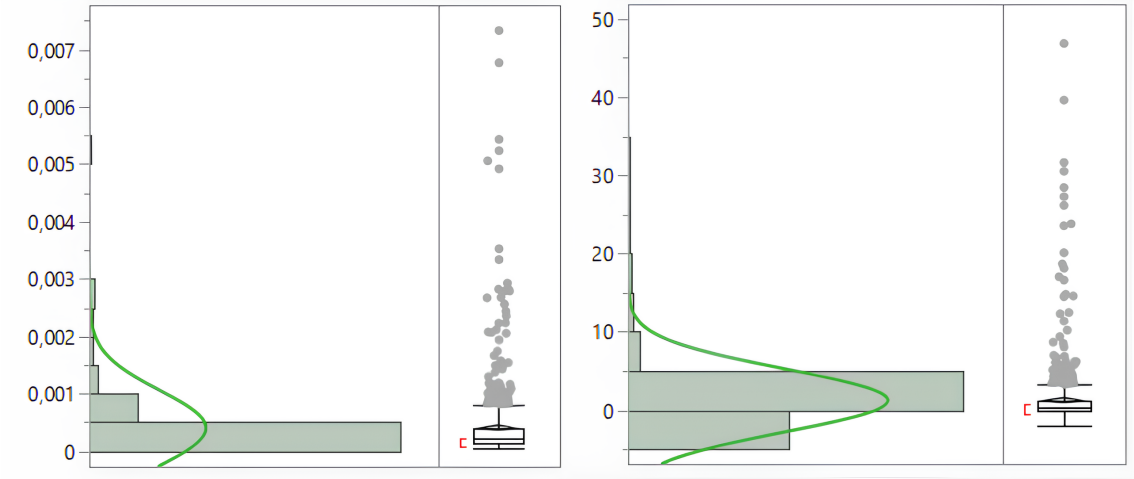


Figure 4.6: Data distribution for mean MI (on the left), and mean z-score (on the right).

For EEG data analysis, in order to explore the differences between ALS patients and healthy controls in Beta-Gamma (12-30 Hz vs 30-100 Hz) mean PAC MI over the EEG channels of interest, a repeated-measure linear mixed-effect model (rmLMM) (ANOVA Full Factorial Design) was constructed, and its specifications can be found in Appendix D. Different models were created:

1. rmLMM for mean MI considering two runs.
2. rmLMM for mean MI considering the average of runs.
3. rmLMM for mean z-score considering two runs.
4. rmLMM for mean z-score considering the average of runs.

A p-value of ≤ 0.05 was considered statistically significant, and a post-hoc analysis was conducted to calculate student's t-test. To assess the effectiveness of the mean MI and determine whether this measure could be used to stratify ALS patients and healthy controls, a receiver operating characteristic (ROC) curve analysis [55] was also carried out using JMP®.

5

Results and Discussion

The first Section of this Chapter is dedicated to the results obtained from the correlations studies performed to evaluate the feasibility of producing surrogate data, in the particular conditions this project presented. The results, which were visualized using *Python*, provide insights into the challenges and limitations encountered with the proposed surrogate data generation methods. The subsections that follow detail the findings for each method tested.

The second Section delves into the findings of rmLMM models applied to both mean MI and mean z-scores derived from PAC analysis. It also covers the subsequent post-hoc and ROC curves analysis, with results generated using JMP®. The following subsections provide a detailed exploration of the different models used to assess the differences between ALS patients and healthy controls.

5.1 Surrogate data production

5.1.1 Circular shifting

To verify the prospect of applying this method, an autocorrelation study was performed. In this, every post stimulus period, i.e., part of each epoch, was correlated with itself to assess its similarity throughout the signal. Results show that, as expected, the autocorrelation is very high within each epoch, as exemplified in Figure 5.1.

This demonstrates that if we were to ignore the portion of the signal highly correlated, in order to safely produce surrogate data by circularly shifting, it would be necessary to discard about 80% of the portion of the signal considered, since it is only after this moment that the correlation drops to less than 0.2.

Given that the main focus lies in the whole extent of the first 100 ms post stimulus, it is clear this methodology cannot be implemented.

5.1.2 Randomised trial shuffling

In turn, to assess the possibility of shuffling amplitudes between different epochs a correlation study between these was conducted. However, when correlating different

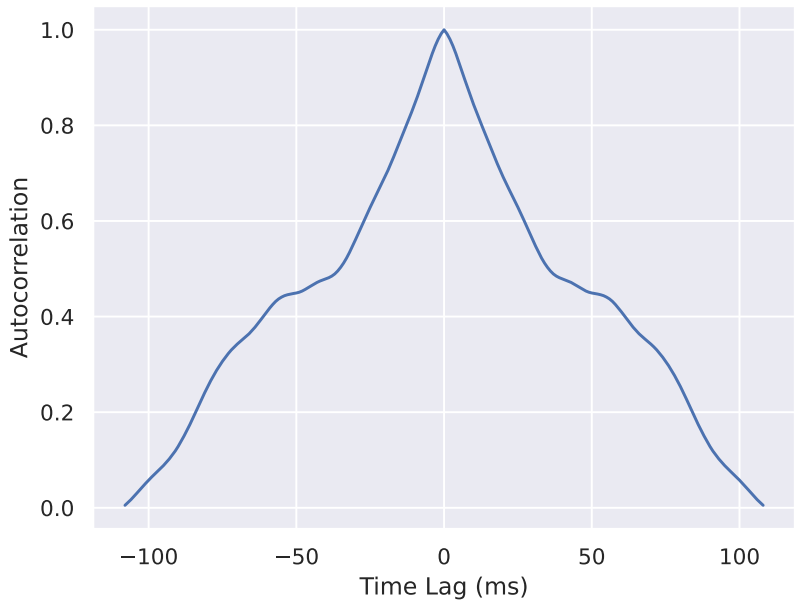


Figure 5.1: Example of autocorrelation of the high-frequency amplitudes envelope, for one epoch, in the 102 ms post stimulus period.

epochs, it became clear that comparing more than 200 epochs was very challenging. Conducting a thorough analysis of all possible shuffling combinations is impractical but, visually, over half of the epochs were significantly correlated, making it risky to use randomised trial shuffling to generate surrogate data. The complexity of this analysis is illustrated in Figure 5.2 where it is possible to see the correlation each epoch presents with the others.

5.1.3 Section discussion

When thinking about surrogate data production through circular shifting it is important to remember that the window of analysis corresponds to only 102 ms. Therefore, this implies that each segment is highly correlated with itself, i.e., with such a short time span, even shifting at a medium point of the envelope would not disrupt the coupling present in the data since the signal's response is very similar both in the beginning and at the end of the period considered.

On the other hand, by stimulating each subject, a SEP is being created. Regretfully, the fact that a stimulus-related potential exists suggests that some frequency components are locked to the stimulation as well as among themselves. This means that even though the brain's response to an external stimulus varies from epoch to epoch, most of these responses will be strikingly similar to one another. Hence, an attempt at randomly shuffling between epochs would not succeed in eliminating PAC and producing surrogate evidence for the null hypothesis, since the similarities between epochs would not be sufficient to disturb the coupling between low frequency phase and high frequency amplitude.

It is clear that the goal with surrogate data is to disrupt the coupling present in the

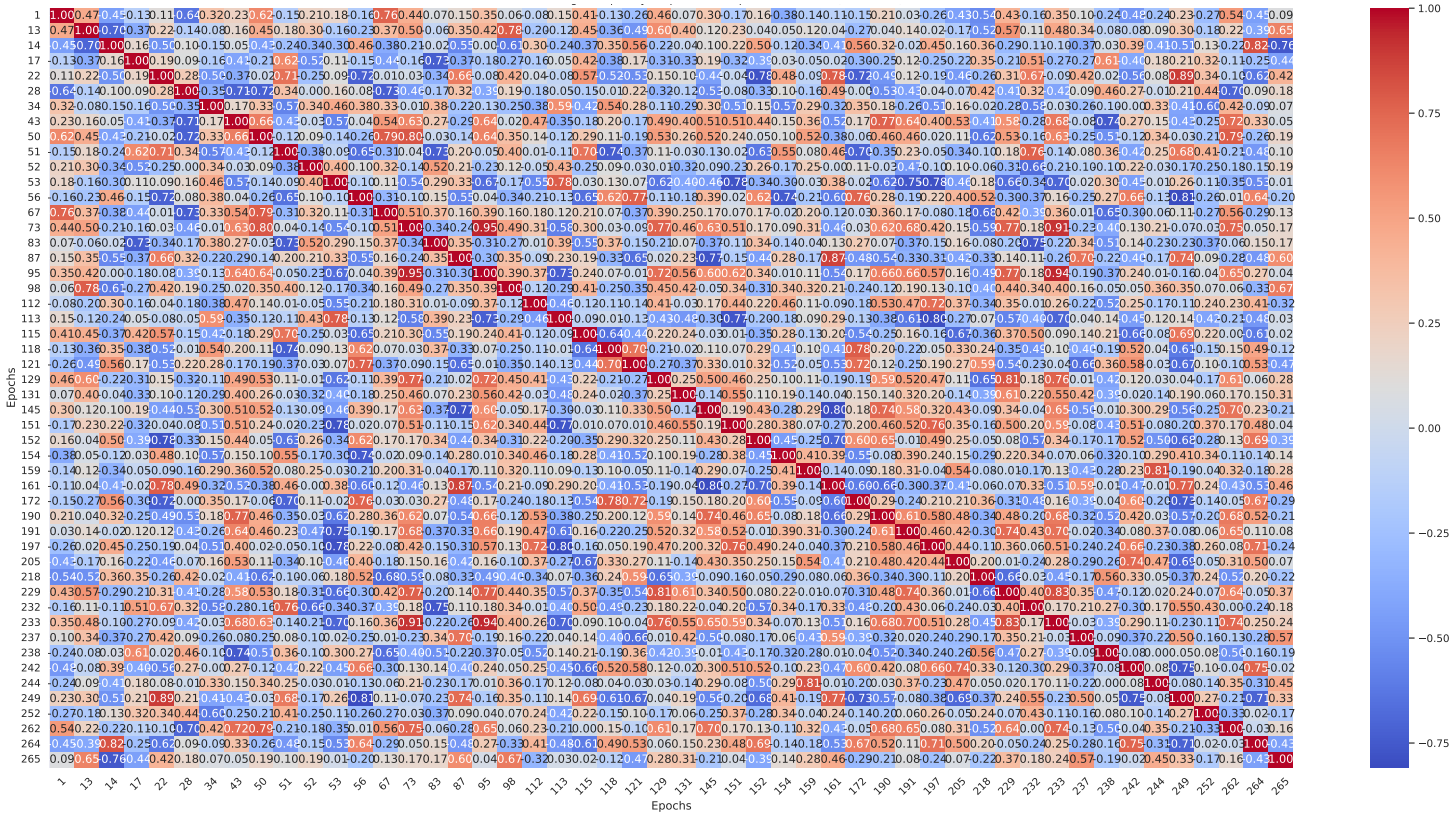


Figure 5.2: Example of a correlation matrix of high-frequency amplitudes envelope between multiple epochs.

data. Nevertheless, methods like circular shifting or randomised trial shuffling could not guarantee this condition. Thus, they were impractical to implement reliably, and without any other viable way to build surrogate data, this approach was discarded for the study in question.

5.2 Statistical analysis of PAC

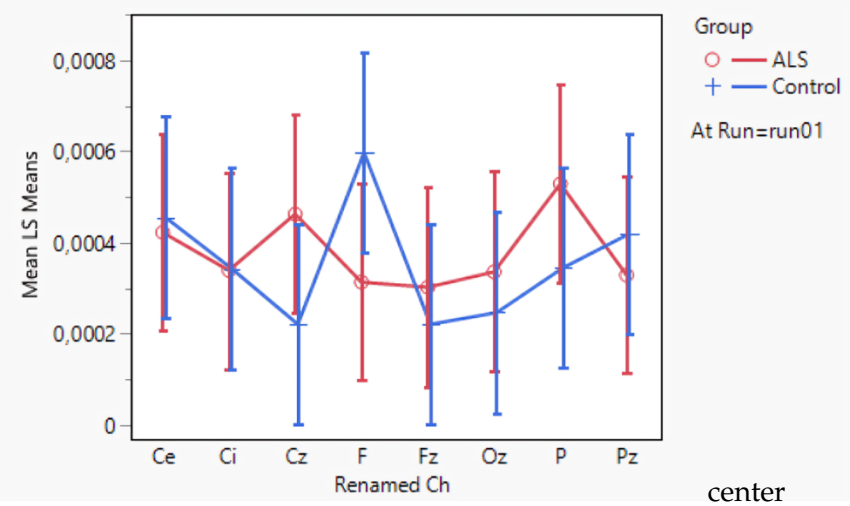
5.2.1 rmLMM for mean MI considering two runs

A first rmLMM was conducted considering the mean MI values of the post stimulus period, for each run recorded. The parameter estimates for this model reveals that the F channel could present significant alterations in ALS group, as seen in Table 5.1. However, a post-hoc analysis for the least square means (LSMeans) of the effects expressed that mean MI over F channel in ALS vs healthy control is not significant, based on student's t test (p-value = 0.1740).

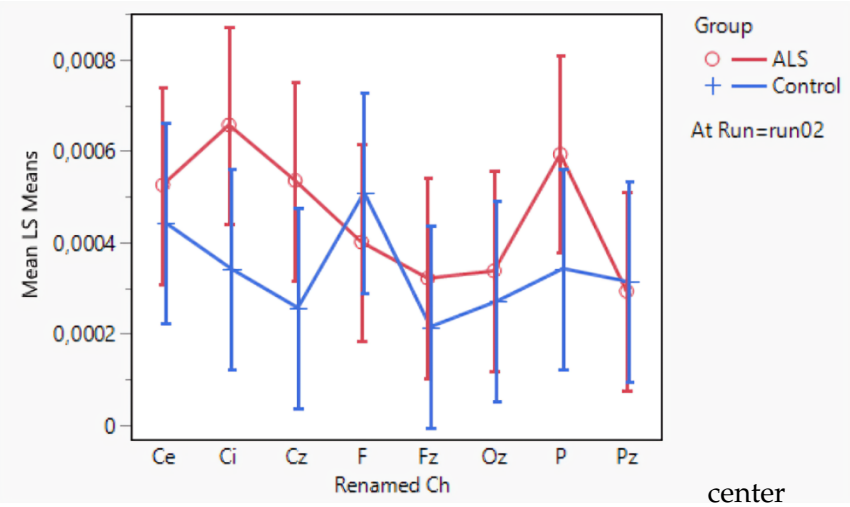
Despite visually being able to detect some differences in ALS group between run 1 and run 2, as the mean MI LSMeans shows in Figure 5.3, when analysing the F test for Run Effect there was no significant difference between runs (p-value of 0.1727), and for that reason, next model took into consideration the average of both runs.

Table 5.1: p-values for the coefficient estimates in the first rmLMM. This considers the interaction between Group and Channel.

	ALS * Ce	ALS * Ci	ALS * Cz	ALS * F	ALS * Fz	ALS * Oz	ALS * P
p-value	0.6679	0.4517	0.0921	0.0160	0.8479	0.9588	0.1919



(a) Mean MI for run 1



(b) Mean MI for run 2

Figure 5.3: LSMeans plot comparing the effects of Group, Channel, and Run.

5.2.2 rmLMM for mean MI considering the average of runs

Secondly, another rmLMM was explored considering the average of the mean MI values from both runs during the post stimulus period. These values are displayed in Table 5.2.

Table 5.2: Average mean MI values across both runs.

Channel	Healthy	ALS	p-value
F	$(5.53 \pm 4.96) \times 10^{-4}$	$(3.57 \pm 3.38) \times 10^{-4}$	0.1114
Fz	$(2.18 \pm 1.21) \times 10^{-4}$	$(2.52 \pm 3.04) \times 10^{-4}$	0.6089
Ce	$(4.49 \pm 5.99) \times 10^{-4}$	$(4.74 \pm 3.87) \times 10^{-4}$	0.8645
Ci	$(3.42 \pm 2.70) \times 10^{-4}$	$(4.98 \pm 4.87) \times 10^{-4}$	0.1763
Cz	$(2.39 \pm 1.24) \times 10^{-4}$	$(9.34 \pm 26.80) \times 10^{-4}$	0.2109
P	$(3.43 \pm 2.00) \times 10^{-4}$	$(5.95 \pm 10.57) \times 10^{-4}$	0.2574
Pz	$(3.66 \pm 3.22) \times 10^{-4}$	$(2.59 \pm 1.45) \times 10^{-4}$	0.1436
Oz	$(2.59 \pm 1.72) \times 10^{-4}$	$(2.77 \pm 1.89) \times 10^{-4}$	0.7214

The parameter estimates for this model reveals that the Cz channel could present significant alterations in ALS group, as seen in Table 5.3. Besides, a post-hoc analysis for the LSMeans of the effects expressed that the averaged mean MI over Cz channel in ALS vs healthy control is significant, based on student's t test (p-value = 0.0026).

Table 5.3: p-values for the coefficient estimates in the second rmLMM. This considers the interaction between Group and Channel.

	ALS * Ce	ALS * Ci	ALS * Cz	ALS * F	ALS * Fz	ALS * Oz	ALS * P
p-value	0.5888	0.8931	0.0038	0.0939	0.8298	0.7680	0.5283

Following, a ROC curve analysis was carried out to evaluate the performance of PAC over Cz, illustrated by Figure 5.4. The findings indicate that the MI did not significantly predict the presence of ALS, as evidenced by the ChiSquare of 2.121248, and the p-value of 0.1453. Plus, the area under the curve (AUC) for the model was 0.43333, suggesting a poor discriminative ability.

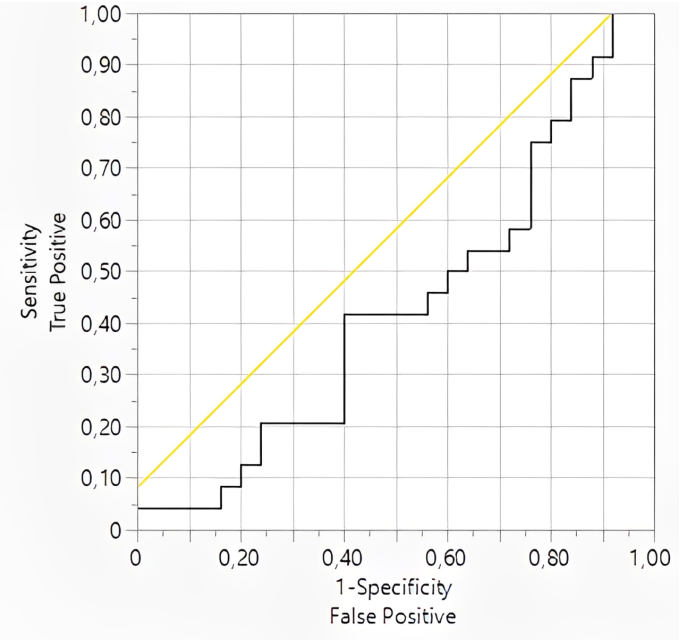


Figure 5.4: ROC curve for Cz channel, considering the averaged mean MI.

Moreover, it is possible to see in Figure 5.5 an increase of the averaged mean MI LSMeans in Cz channel for ALS group as compared to healthy control group.

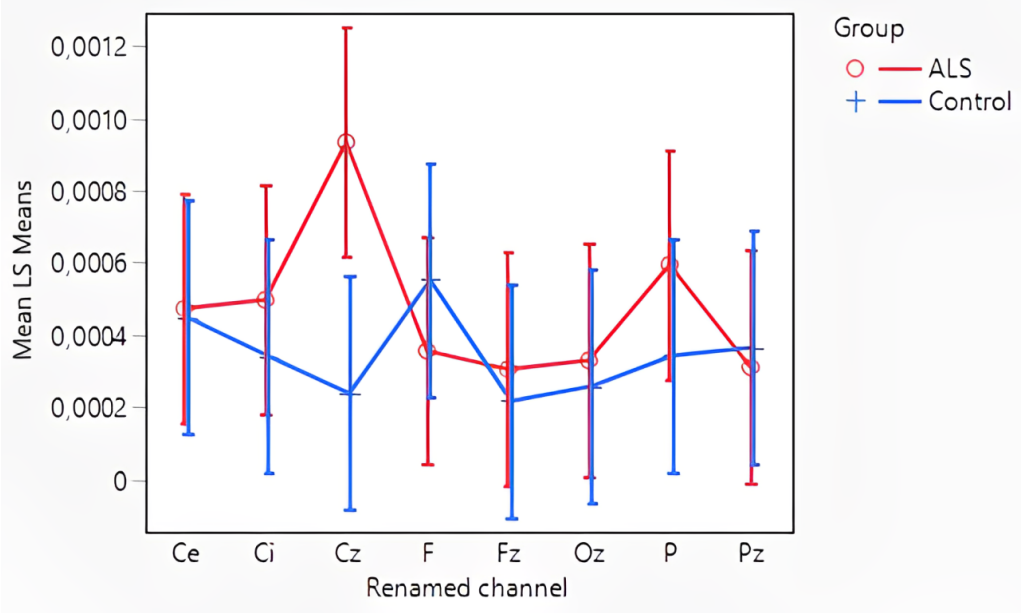


Figure 5.5: The averaged mean MI values are plotted against the effects of Group and Channel using an LSMeans plot.

5.2.3 rmLMM for mean z-score in two runs

In order to take into consideration the pre-stimulus period and establish a relationship between the pre- and the post-, a comodulogram of z-scores, as opposed to MI values, was built. Consequently, a new rmLMM was investigated to see the behaviour of the data, on both runs individually. The parameter estimates for this model reveals that the Cz channel could present significant alterations in ALS group, as seen in Table 5.4. Plus, a post-hoc analysis for the LSMeans of effects expressed that the mean z-score over Cz channel in ALS vs healthy control is significant, based on student's t test (p-value = 0.0474).

Table 5.4: p-values for the coefficient estimates in the third rmLMM. This considers the interaction between Group and Channel.

	ALS * Ce	**ALS * Ci**	**ALS * Cz**	**ALS * F**	**ALS * Fz**	**ALS * Oz**	**ALS * P**
p-value	0.5882	0.9673	0.0431	0.6461	0.9281	0.3682	0.6872

After, a ROC curve analysis was executed to evaluate the performance of PAC over Cz, illustrated by Figure 5.6. Results show that the z-score of the MI was not a significant predictor of ALS status, with a ChiSquare of 1.005462, a p-value of 0.3160, and an AUC for the model of 0.46684. Although there has been a slight improvement from the prior ROC analysis, the discriminative capacity remains unsatisfactory.

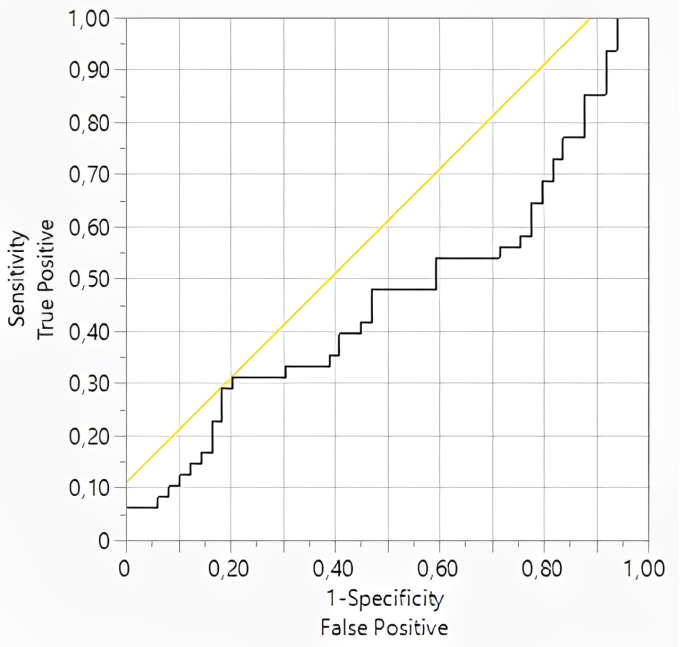


Figure 5.6: ROC curve for Cz channel, considering the mean z-score.

Once again there is no significant disparity between runs (p-value of 0.3861), what can be visually confirmed by Figure 5.7. Following this result, a final model was produced averaging both runs.

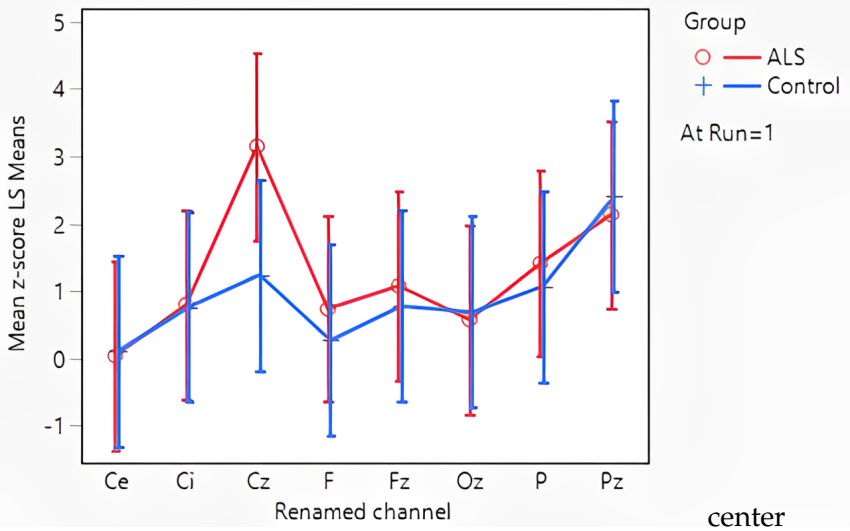
5.2.4 rmLMM for mean z-score with average of runs

Finally, a rmLMM was explored using the average of the mean z-scores from both runs during the post stimulus period. These values are displayed in Table 5.5.

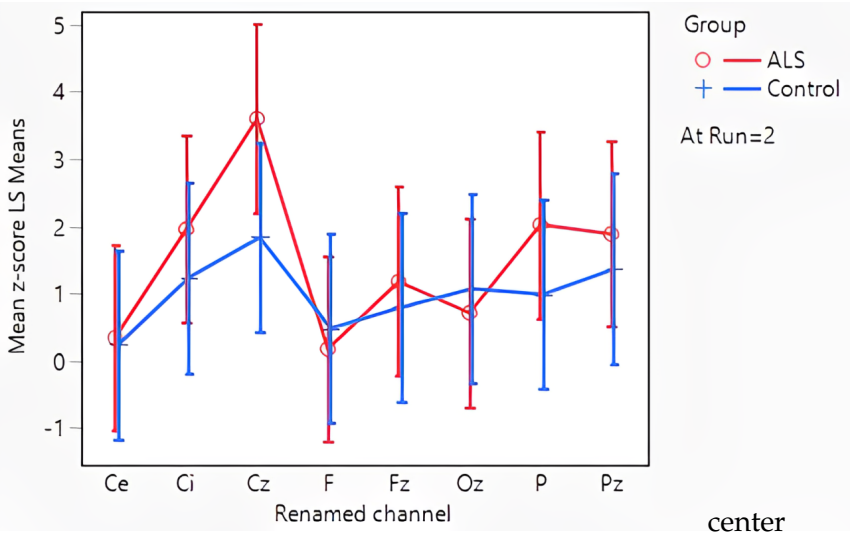
Table 5.5: Average mean z-score values across both runs.

Channel	Healthy	ALS	p-value
F	0.37 ± 0.79	0.46 ± 1.10	0.7659
Fz	0.78 ± 1.09	0.76 ± 0.92	0.9211
Ce	0.36 ± 1.20	0.29 ± 1.39	0.8640
Ci	1.00 ± 1.88	1.68 ± 3.95	0.4478
Cz	1.53 ± 2.54	2.11 ± 7.12	0.7110
P	1.03 ± 1.41	1.72 ± 3.88	0.4171
Pz	1.88 ± 3.08	2.01 ± 3.88	0.8986
Oz	0.88 ± 1.43	0.27 ± 0.50	0.0575

The parameter estimates for this model reveals that no channel presents significant alterations in ALS group, as it can be seen Table 5.6, thus no post-hoc analysis was carried out.



(a) Mean z-score for run 1



(b) Mean z-score for run 2

Figure 5.7: LSMeans plot comparing the effects of Group, Channel, and Run.

Table 5.6: p-values for the coefficient estimates in the fourth rmLMM. This considers the interaction between Group and Channel.

	ALS * Ce	**ALS * Ci**	**ALS * Cz**	**ALS * F**	**ALS * Fz**	**ALS * Oz**	**ALS * P**
p-value	0.5289	0.5238	0.5554	0.7026	0.8391	0.4440	0.5164

Furthermore, it is possible to see in Figure 5.8 that there is no obvious difference between groups in the mean z-score LSMeans for all channels.

5.2.5 Section discussion

Despite the common use of surrogate data to validate PAC results, there are cases where is valid to study PAC without surrogate production, as the case of studies where two conditions are being compared [56], or in a more exploratory stage of research when

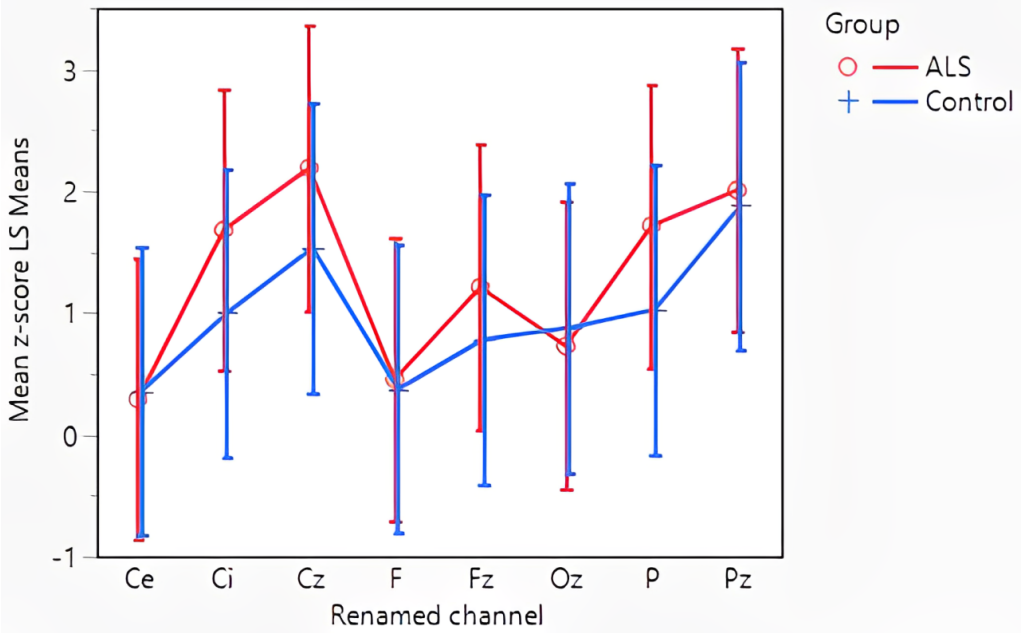


Figure 5.8: The averaged mean z-scores are plotted against the effects of Group and Channel using an LSMeans plot.

there are limited resources to compute surrogate given its complexity. In this project, the initial models were conducted without comparisons, simply studying the raw findings to identify any potential significance; this approach was chosen due to the inherent evoked response in stimulated data. On the other hand, the subsequent models tried to establish a comparison between pre- and post-stimulus condition by calculating the z-score.

By doing a rmLMM the goal is to find differences in between the two groups - ALS patients and healthy controls. To achieve that, a channel by channel analysis was performed in the area of interest in the brain. This revealed some differences, mainly in Cz channel as the plots shown, leading to a post-hoc analysis in which the objective was to analyse student's t-tests in between different pairs of channels, mainly the ones where there could possibly be a significant alteration in between ALS group and healthy controls.

The first model, conducted using the two runs of signal recorded, indicated no significant distinction between the ALS and control group in any of the channels. Plus, even though there was no substantial difference between runs, which permitted the building of the next model, it was still possible to visually witness a distinct response to stimulation in ALS group on run 2 which was higher compared to run 1. However, due to the experimental procedure where different stimulation intensities were applied in random order to each subject, it is impossible to draw specific conclusions. This difference could result from brain habituation to the stimulation or slight accumulation of brain basal activity, particularly since the most significant changes occur around the central channels. Nevertheless, as the two runs were not conducted consecutively it is only possible to speculate, rather than draw any definitive conclusions.

On a second version of the model, where the two runs were averaged together, the

mean values showed that while there is an increase in activity in most channels, the mean MI values are decreasing, from healthy controls to ALS patients, in just a couple of them. Nevertheless, only Cz channel manifests a significant alteration as it can be visually interpreted, leading to the evaluation of a ROC curve that did not produce satisfactory results. The fact that the AUC was only approximately 43% indicates, from a clinical standpoint, that the selected measure is not very effective in discriminating between patients and controls.

Examining the third model — the first to take each run's mean z-score into account — a significant difference was found for the Cz channel in both runs. After that, a ROC curve was computed, and while it showed a marginally improved response over the previous one, the AUC did not even reach 50%, which was still unsatisfactory. Furthermore, even though there was a little increase in mean z-score on central channels for ALS groups between runs 1 and 2, the response was more consistent throughout runs. This suggests that rather than relying just on the raw post-stimulus results, evaluating the z-score of the data — which takes into account both the before and after stimulus — is probably a more appropriate or reliable technique.

Finally, an average of the two runs was performed, where the resultant values could be observed. Here, an elevated standard deviation was seen, indicating a high degree of measure dispersion. However, it also allowed for the verification of a change from the previous observation of average values in the second model, where only a few channels in the ALS group showed depression; now, nevertheless, those same channels show an increase. Anyway, when comparing group with channel, no significant difference could be found, leading to the conclusion of the analysis with no further noteworthy outcomes.

Ergo, none of the results offered by the models or consequent analysis manifest PAC MI as suitable to discriminate between ALS and healthy groups. Notwithstanding the findings, there are a few other points to bare in mind.

Given that the active area following stimulation is the sensorimotor area, the hypothesis was that the main changes would occur over the sensorimotor area, mainly C3/C4 and C5/C6, rather than in the centre of the interhemispheric sulcus, as is verified. This could be due to the high activity resultant from the stimulation or, just by the fact that PAC is not a good method to apply in stimulated data.

6

Conclusions

6.1 Main conclusions

This project's main goal was to find a highly precise measure for detecting a biomarker of cortical dysfunctions at an early stage of ALS, by computing PAC in stimulated EEG data. In order to do this, a preprocessing pipeline was initially created, allowing the data to be cleaned before being submitted to an analytical pipeline for PAC, where the mean MI was extracted for posterior analysis.

One of the objectives' key conclusion was that, unlike earlier work done in a resting condition, it was not viable to construct surrogate data using this particular dataset. This limitation made it impossible to adapt the existing pipeline for studying PAC, suggesting the need for a different strategy.

Once PAC measures were retrieved, a different objective was pursued: attempting to identify differences between the two subject groups. However, the findings did not fully support the initial hypothesis. The analysis revealed that beta-gamma PAC performed on stimulated data did not provide satisfactory diagnostic accuracy, contrary to what had been observed in resting-state data. This suggests that the dynamics of brain activity during stimulation might differ substantially from those during rest, affecting the reliability of PAC as a biomarker in this context.

Moreover, the conducted PAC analysis produced little biological understanding of how the brain functions post stimulation. The absence of extra data highlights how difficult it is to understand PAC in stimulated situations and raises the possibility that the approach may not be as instructive as first thought.

On a broader overview, the main goal of this project was achieved as the proposed analysis, and the necessary framework, were completed, enabling data assessment. However, the primary hypothesis was not supported, and PAC analysis of stimulated data was unable to distinguish between healthy controls and ALS patients.

In conclusion, while the project succeeded in developing and implementing a robust analytical framework, the findings suggest that PAC analysis of stimulated EEG data does not provide a viable diagnostic tool for early-stage ALS. This outcome directs future

research toward focusing on resting-state data, where PAC has shown greater promise in previous studies.

6.2 Limitations

The fundamental drawback of this dissertation was its extremely constrained analysis window. This limitation significantly impacted the feasibility of producing surrogate data, which is a critical component in validating the statistical significance of PAC analyses. Without the ability to generate surrogate data, the analytical process became more complex and less reliable, as it was challenging to ascertain whether the observed PAC findings were genuinely significant.

Moreover, the restricted time response of the SEP further compounded the problem. SEPs typically have a brief response period, which in this study, reduced the duration over which meaningful data could be analysed. This short time window hampered a more extended analysis that could have yielded deeper insights into the brain's response to stimuli. Consequently, there was no way to explore the lower theta frequency spectrum in this constrained amount of time, fact that is particularly important because previous studies have demonstrated that theta-gamma PAC exhibits substantial differences when comparing healthy subjects and patients with ALS disease.

The inability to explore the lower theta frequency band due to the SEP's limited response time meant that a potentially valuable aspect of the PAC analysis was left unexplored. Missing out on this analysis might have overlooked crucial differences in brain activity that could have provided a more comprehensive understanding of the neurophysiological distinctions between the ALS patients and healthy controls studied.

To summarise, the limited analytical window resulting from the restricted time response of the SEP presented considerable obstacles for this dissertation. These limitations hindered the generation of surrogate data and precluded a thorough examination of other lower frequency bands, which in turn complicated the analytical procedure and potentially have made an impact on the reliability and relevance of the results.

6.3 Future work

Although the study concluded that there is little physiological interest in examining beta-gamma PAC using stimulated data, there are several additional considerations that could impact the analysis procedure and potentially enhance future research outcomes.

One area for future investigation is the variation in stimulation intensities. Instead of relying solely on intensities that are six times the PT, exploring a broader range of stimulation intensities might provide different insights as lower or varying intensities could reduce the likelihood of brain adaptation to the stimulation.

Another consideration is the selective analysis of epochs. Rather than averaging the mean MI across all recorded epochs, future studies could benefit from analysing each epoch individually. This approach allows for the identification and exclusion of outlier epochs that might disproportionately influence the final outcomes.

On another note, both the time-frequency analysis (as detailed in Appendix B) and a previous study conducted to examine the data on this same dataset, [49], show that there is a reaction from the brain following peripheral nerve stimulation. This suggests that, even if PAC is not the ideal technique for analysing this type of data, alternative methodologies could be developed to investigate brain feedback more effectively.

Bibliography

[1] J. M. Lourenço. *The NOVAthesis LaTeX Template User's Manual*. NOVA University Lisbon. 2021. URL: https://github.com/joaomlourenco/novathesis/raw/main/template.pdf (cit. on p. i).

[2] O. Hardiman et al. "Amyotrophic lateral sclerosis". In: *Nature Reviews Disease Primers* 3.1 (2017-10), p. 17071. ISSN: 2056-676X. DOI: 10.1038/nrdp.2017.71. URL: https://www.nature.com/articles/nrdp201771 (cit. on pp. 1, 2).

[3] R. H. Brown and A. Al-Chalabi. "Amyotrophic Lateral Sclerosis". In: *New England Journal of Medicine* 377.2 (2017-07). Ed. by D. L. Longo, pp. 162–172. ISSN: 0028-4793. DOI: 10.1056/NEJMra1603471. URL: http://www.nejm.org/doi/10.1056/NEJMra1603471 (cit. on pp. 1, 2).

[4] P. Masrori and P. Van Damme. "Amyotrophic lateral sclerosis: a clinical review". In: *European Journal of Neurology* 27.10 (2020-10), pp. 1918–1929. ISSN: 1351-5101. DOI: 10.1111/ene.14393. URL: https://onlinelibrary.wiley.com/doi/10.1111/ene.14393 (cit. on pp. 1, 2).

[5] A. Eisen. "The Dying Forward Hypothesis of ALS: Tracing Its History". In: *Brain Sciences* 11.3 (2021-02), p. 300. ISSN: 2076-3425. DOI: 10.3390/brainsci11030300. URL: https://www.mdpi.com/2076-3425/11/3/300 (cit. on p. 3).

[6] S. K. Vaughan et al. "Degeneration of proprioceptive sensory nerve endings in mice harboring amyotrophic lateral sclerosis–causing mutations". In: *Journal of Comparative Neurology* 523.17 (2015-12), pp. 2477–2494. ISSN: 0021-9967. DOI: 10.1002/cne.23848. URL: https://onlinelibrary.wiley.com/doi/10.1002/cne.23848 (cit. on p. 3).

[7] S. Vucic. "Novel threshold tracking techniques suggest that cortical hyperexcitability is an early feature of motor neuron disease". In: *Brain* 129.9 (2006-09), pp. 2436–2446. ISSN: 0006-8950. DOI: 10.1093/brain/awl172. URL: https://academic.oup.com/brain/article-lookup/doi/10.1093/brain/awl172 (cit. on p. 3).

[8] S. Vucic, G. A. Nicholson, and M. C. Kiernan. "Cortical hyperexcitability may precede the onset of familial amyotrophic lateral sclerosis". In: *Brain* 131.6 (2008-06), pp. 1540–1550. ISSN: 1460-2156. DOI: 10.1093/brain/awn071. URL: https://academic.oup.com/brain/article-lookup/doi/10.1093/brain/awn071 (cit. on p. 3).

[9] J. Scekic-Zahirovic et al. *Cortical hyperexcitability in mouse models and patients with amyotrophic lateral sclerosis is linked to noradrenaline deficiency*. Tech. rep. 2024, p. 3665. URL: https://www.science.org (cit. on pp. 4, 10, 15, 16).

[10] R. Tatti et al. "Neurophysiology and Regulation of the Balance Between Excitation and Inhibition in Neocortical Circuits". In: *Biological Psychiatry* 81.10 (2017-05), pp. 821–831. ISSN: 00063223. DOI: 10.1016/j.biopsych.2016.09.017. URL: https://linkinghub.elsevier.com/retrieve/pii/S0006322316328530 (cit. on p. 7).

[11] M. Mattson. "Excitotoxicity". In: *Stress: Physiology, Biochemistry, and Pathology*. Elsevier, 2019, pp. 125–134. DOI: 10.1016/B978-0-12-813146-6.00011-4 (cit. on p. 7).

[12] B. Flanagan et al. "A computational study of astrocytic glutamate influence on post-synaptic neuronal excitability". In: *PLOS Computational Biology* 14.4 (2018-04), e1006040. ISSN: 1553-7358. DOI: 10.1371/journal.pcbi.1006040 (cit. on p. 7).

[13] M. Xie et al. *Regulation of cortical hyperexcitability in amyotrophic lateral sclerosis: focusing on glial mechanisms*. 2023-12. DOI: 10.1186/s13024-023-00665-w (cit. on pp. 7, 8, 13).

[14] M. P. Cruz. "Edaravone (Radicava): A Novel Neuroprotective Agent for the Treatment of Amyotrophic Lateral Sclerosis." In: *P & T : a peer-reviewed journal for formulary management* 43.1 (2018-01), pp. 25–28. ISSN: 1052-1372. URL: http://www.ncbi.nlm.nih.gov/pubmed/29290672%20http://www.pubmedcentral.nih.gov/articlerender.fcgi?artid=PMC5737249 (cit. on p. 7).

[15] S. Vucic et al. "Cortical hyperexcitability: Diagnostic and pathogenic biomarker of ALS". In: *Neuroscience Letters* 759 (2021-08). ISSN: 18727972. DOI: 10.1016/j.neulet.2021.136039 (cit. on p. 7).

[16] P. Menon et al. "Cortical hyperexcitability evolves with disease progression in ALS". In: *Annals of Clinical and Translational Neurology* 7.5 (2020-05), pp. 733–741. ISSN: 23289503. DOI: 10.1002/acn3.51039 (cit. on p. 8).

[17] M. X. Cohen. *Analyzing Neural Time Series Data: Theory and Practice*. 1st. Cambridge, Massachusetts: The MIT Press, 2014-01. ISBN: 9780262019873 (cit. on p. 8).

[18] S. R. Passmore et al. "The origin, and application of somatosensory evoked potentials as a neurophysiological technique to investigate neuroplasticity". In: *J Can Chiropr Assoc* 58.2 (2014). ISSN: 1715-6181 (cit. on pp. 8, 9, 14).

[19] C. Iglesias et al. "Electrophysiological and spinal imaging evidences for sensory dysfunction in amyotrophic lateral sclerosis". In: *BMJ Open* 5.2 (2015). ISSN: 20446055. DOI: 10.1136/bmjopen-2015-007659 (cit. on p. 9).

[20] B. Cengiz et al. "Excitability of somatosensory cortex is increased in ALS: A SEP recovery function study". In: *Clinical Neurophysiology* 155 (2023-11), pp. 58–64. ISSN: 18728952. DOI: 10.1016/j.clinph.2023.08.013 (cit. on pp. 9, 19).

[21] P. A. Theys, E. Peeters, and W. Robberecht. "Evolution of motor and sensory deficits in amyotrophic lateral sclerosis estimated by neurophysiological techniques". In: *Journal of Neurology* 246.6 (1999-06), pp. 438–442. ISSN: 0340-5354. DOI: 10.1007/s004150050379. URL: http://link.springer.com/10.1007/s004150050379 (cit. on p. 9).

[22] A. C. Onslow, R. Bogacz, and M. W. Jones. "Quantifying phase-amplitude coupling in neuronal network oscillations". In: *Progress in Biophysics and Molecular Biology* 105.1-2 (2011-03), pp. 49–57. ISSN: 00796107. DOI: 10.1016/j.pbiomolbio.2010.09.007 (cit. on pp. 9, 10).

[23] R. T. Canolty and R. T. Knight. *The functional role of cross-frequency coupling*. 2010-11. DOI: 10.1016/j.tics.2010.09.001 (cit. on p. 10).

[24] A. Von Stein and J. Sarnthein. *Different frequencies for different scales of cortical integration: from local gamma to long range alphartheta synchronization*. Tech. rep. 2000, p. 301313 (cit. on p. 10).

[25] A. B. Tort et al. "Measuring phase-amplitude coupling between neuronal oscillations of different frequencies". In: *Journal of Neurophysiology* 104.2 (2010), pp. 1195–1210. ISSN: 15221598. DOI: 10.1152/jn.00106.2010 (cit. on pp. 10, 11, 23).

[26] A. B. L. Tort et al. *Dynamic cross-frequency couplings of local field potential oscillations in rat striatum and hippocampus during performance of a T-maze task*. Tech. rep. 2008. URL: www.pnas.org/cgi/content/full/ (cit. on pp. 11, 12, 22, 61, 62).

[27] S. Vucic et al. "Utility of threshold tracking transcranial magnetic stimulation in ALS". In: *Clinical Neurophysiology Practice* 3 (2018), pp. 164–172. ISSN: 2467981X. DOI: 10.1016/j.cnp.2018.10.002. URL: https://doi.org/10.1016/j.cnp.2018.10.002%20https://linkinghub.elsevier.com/retrieve/pii/S2467981X18300301 (cit. on p. 13).

[28] H. Tankisi et al. "Conventional and threshold-tracking transcranial magnetic stimulation tests for single-handed operation". In: *Journal of Visualized Experiments* 2021.174 (2021). ISSN: 1940087X. DOI: 10.3791/62787 (cit. on p. 13).

[29] K. R. Mills. "The natural history of central motor abnormalities in amyotrophic lateral sclerosis". In: *Brain* 126.11 (2003-11), pp. 2558–2566. ISSN: 1460-2156. DOI: 10.1093/brain/awg260. URL: https://academic.oup.com/brain/article-lookup/doi/10.1093/brain/awg260 (cit. on p. 13).

[30] A. G. Floyd et al. "Transcranial magnetic stimulation in ALS". In: *Neurology* 72.6 (2009-02), pp. 498–504. ISSN: 0028-3878. DOI: 10.1212/01.wnl.0000341933.97883.a4. URL: https://www.neurology.org/doi/10.1212/01.wnl.0000341933.97883.a4 (cit. on p. 13).

[31] P. Menon et al. "Sensitivity and specificity of threshold tracking transcranial magnetic stimulation for diagnosis of amyotrophic lateral sclerosis: A prospective study". In: *The Lancet Neurology* 14.5 (2015-05), pp. 478–484. ISSN: 14744465. DOI: 10.1016/S1474-4422(15)00014-9 (cit. on p. 13).

[32] M. R. Turner, F. Agosta, and V. Govind. "Neuroimaging in amyotrophic lateral sclerosis R eview". In: 1 (2012), pp. 319–337. DOI: 10.2217/bmm.12.26 (cit. on pp. 13, 14).

[33] E. Verstraete and B. R. Foerster. "Neuroimaging as a New Diagnostic Modality in Amyotrophic Lateral Sclerosis". In: *Neurotherapeutics* 12.2 (2015-04), pp. 403–416. ISSN: 18787479. DOI: 10.1007/s13311-015-0347-9. URL: https://linkinghub.elsevier.com/retrieve/pii/S1878747923008358 (cit. on p. 14).

[34] G. Buzśaki and X. J. Wang. *Mechanisms of gamma oscillations*. 2012-07. DOI: 10.1146/annurev-neuro-062111-150444 (cit. on p. 14).

[35] S. Keeley, A. A. Fenton, and J. Rinzel. "Modeling fast and slow gamma oscillations with interneurons of different subtype". In: *Journal of Neurophysiology* 117.3 (2017-03), pp. 950–965. ISSN: 0022-3077. DOI: 10.1152/jn.00490.2016 (cit. on p. 14).

[36] C. Alvarado-Rojas et al. "Probing cortical excitability using cross-frequency coupling in intracranial EEG recordings: A new method for seizure prediction". In: *Proceedings of the Annual International Conference of the IEEE Engineering in Medicine and Biology Society, EMBS*. 2011, pp. 1632–1635. ISBN: 9781424441211. DOI: 10.1109/IEMBS.2011.6090471 (cit. on p. 14).

[37] C. de Hemptinne et al. "Exaggerated phase–amplitude coupling in the primary motor cortex in Parkinson disease". In: *Proceedings of the National Academy of Sciences* 110.12 (2013-03), pp. 4780–4785. ISSN: 0027-8424. DOI: 10.1073/pnas.1214546110. URL: https://pnas.org/doi/full/10.1073/pnas.1214546110 (cit. on p. 14).

[38] A. Devergnas et al. "Cortical Phase–Amplitude Coupling in a Progressive Model of Parkinsonism in Nonhuman Primates". In: *Cerebral Cortex* 29.1 (2019-01), pp. 167–177. ISSN: 1047-3211. DOI: 10.1093/cercor/bhx314. URL: https://academic.oup.com/cercor/article/29/1/167/4668704 (cit. on p. 14).

[39] A. Ahnaou et al. "Emergence of early alterations in network oscillations and functional connectivity in a tau seeding mouse model of Alzheimer's disease pathology". In: *Scientific Reports* 7.1 (2017-10), p. 14189. ISSN: 2045-2322. DOI: 10.1038/s41598-017-13839-6. URL: https://www.nature.com/articles/s41598-017-13839-6 (cit. on p. 14).

[40] M. S. Goodman et al. "Theta-Gamma Coupling and Working Memory in Alzheimer's Dementia and Mild Cognitive Impairment". In: *Frontiers in Aging Neuroscience* 10.APR (2018-04). ISSN: 1663-4365. DOI: 10.3389/fnagi.2018.00101. URL: http://journal.frontiersin.org/article/10.3389/fnagi.2018.00101/full (cit. on p. 14).

[41] R. Goutagny et al. "Alterations in hippocampal network oscillations and theta–gamma coupling arise before <scp>Aβ</scp> overproduction in a mouse model of <scp>A</scp> lzheimer's disease". In: *European Journal of Neuroscience* 37.12 (2013-06), pp. 1896–1902. ISSN: 0953-816X. DOI: 10.1111/ejn.12233. URL: https://onlinelibrary.wiley.com/doi/10.1111/ejn.12233 (cit. on p. 14).

[42] C. S. Musaeus et al. "Electroencephalographic Cross-Frequency Coupling as a Sign of Disease Progression in Patients With Mild Cognitive Impairment: A Pilot Study". In: *Frontiers in Neuroscience* 14 (2020-08). ISSN: 1662-453X. DOI: 10.3389/fnins.2020.00790. URL: https://www.frontiersin.org/article/10.3389/fnins.2020.00790/full (cit. on p. 14).

[43] L. E. Hughes et al. "Reorganization of cortical oscillatory dynamics underlying disinhibition in frontotemporal dementia". In: *Brain* 141.8 (2018-08), pp. 2486–2499. ISSN: 0006-8950. DOI: 10.1093/brain/awy176 (cit. on p. 14).

[44] J. Aru et al. *Untangling cross-frequency coupling in neuroscience*. 2015-04. DOI: 10.1016/j.conb.2014.08.002 (cit. on pp. 15, 22).

[45] T. Dupré la Tour et al. "Non-linear auto-regressive models for cross-frequency coupling in neural time series". In: *PLoS Computational Biology* 13.12 (2017-12). ISSN: 15537358. DOI: 10.1371/journal.pcbi.1005893 (cit. on p. 15).

[46] A. Er et al. "Extracting transient phase-amplitude coupling from resting-state EEG signals". In: *Proceedings of the IEEE Engineering in Medicine and Biology Society (EMBS), 46th Annual International Conference of the IEEE Engineering in Medicine and Biology Society (EMBS)*. Orlando, Florida, 2024-07 (cit. on pp. 15, 22).

[47] A. Gramfort. "MEG and EEG data analysis with MNE-Python". In: *Frontiers in Neuroscience* 7.7 DEC (2013). ISSN: 1662453X. DOI: 10.3389/fnins.2013.00267. URL: http://journal.frontiersin.org/article/10.3389/fnins.2013.00267/abstract (cit. on p. 17).

[48] S. Sangari et al. "Abnormal cortical brain integration of somatosensory afferents in ALS". In: *Clinical Neurophysiology* 129.4 (2018-04), pp. 874–884. ISSN: 18728952. DOI: 10.1016/j.clinph.2017.12.008 (cit. on pp. 19, 21).

[49] S. Hssain-Khalladi et al. "Further characterisation of late somatosensory evoked potentials using electroencephalogram and magnetoencephalogram source imaging". In: *European Journal of Neuroscience* (2024-07). ISSN: 14609568. DOI: 10.1111/ejn.16379 (cit. on pp. 19, 21, 23, 39).

[50] F. Ranieri et al. "Sensorimotor integration within the primary motor cortex by selective nerve fascicle stimulation". In: *The Journal of Physiology* 600.6 (2022-03), pp. 1497–1514. ISSN: 0022-3751. DOI: 10.1113/JP282259. URL: https://physoc.onlinelibrary.wiley.com/doi/10.1113/JP282259 (cit. on p. 19).

[51] S. Sangari et al. "Impairment of sensory-motor integration at spinal level in amyotrophic lateral sclerosis". In: *Clinical Neurophysiology* 127.4 (2016-04), pp. 1968–1977. ISSN: 18728952. DOI: 10.1016/j.clinph.2016.01.014 (cit. on p. 21).

[52] M. Illman et al. "Reproducibility of Rolandic beta rhythm modulation in MEG and EEG". In: *Journal of Neurophysiology* 127.2 (2022-02), pp. 559–570. ISSN: 0022-3077. DOI: 10.1152/jn.00267.2021. URL: https://journals.physiology.org/doi/10.1152/jn.00267.2021 (cit. on p. 23).

[53] W. Gaetz and D. Cheyne. "Localization of sensorimotor cortical rhythms induced by tactile stimulation using spatially filtered MEG". In: *NeuroImage* 30.3 (2006-04), pp. 899–908. ISSN: 10538119. DOI: 10.1016/j.neuroimage.2005.10.009. URL: https://linkinghub.elsevier.com/retrieve/pii/S1053811905007858 (cit. on p. 23).

[54] E. Houdayer et al. "Relationship between event-related beta synchronization and afferent inputs: Analysis of finger movement and peripheral nerve stimulations". In: *Clinical Neurophysiology* 117.3 (2006-03), pp. 628–636. ISSN: 13882457. DOI: 10.1016/j.clinph.2005.12.001. URL: https://linkinghub.elsevier.com/retrieve/pii/S1388245705004803 (cit. on p. 23).

[55] S. Parodi et al. "The clinical meaning of the area under a receiver operating characteristic curve for the evaluation of the performance of disease markers". In: *Epidemiology and Health* 44 (2022). ISSN: 20927193. DOI: 10.4178/epih.e2022088 (cit. on p. 25).

[56] J. Scekic-Zahirovic et al. "Cortical hyperexcitability in mouse models and patients with amyotrophic lateral sclerosis is linked to noradrenaline deficiency". In: *Science Translational Medicine* 16.738 (2024-03). ISSN: 1946-6234. DOI: 10.1126/scitranslmed.adg3665. URL: https://www.science.org/doi/10.1126/scitranslmed.adg3665 (cit. on p. 34).

[57] D. Tanner, K. Morgan-Short, and S. J. Luck. "How inappropriate high-pass filters can produce artifactual effects and incorrect conclusions in ERP studies of language and cognition". In: *Psychophysiology* 52.8 (2015-08), pp. 997–1009. ISSN: 0048-5772. DOI: 10.1111/psyp.12437. URL: https://onlinelibrary.wiley.com/doi/10.1111/psyp.12437 (cit. on p. 58).

A

EEG PREPROCESSING STAGES

This appendix contains detailed information about the preprocessing pipeline used to clean the EEG recordings. Each section illustrates a single stage of the process.

A.1 Raw signal

Firstly, it is presented the raw signal (see Figure A.1), after recording, and without any type of procedure applied.

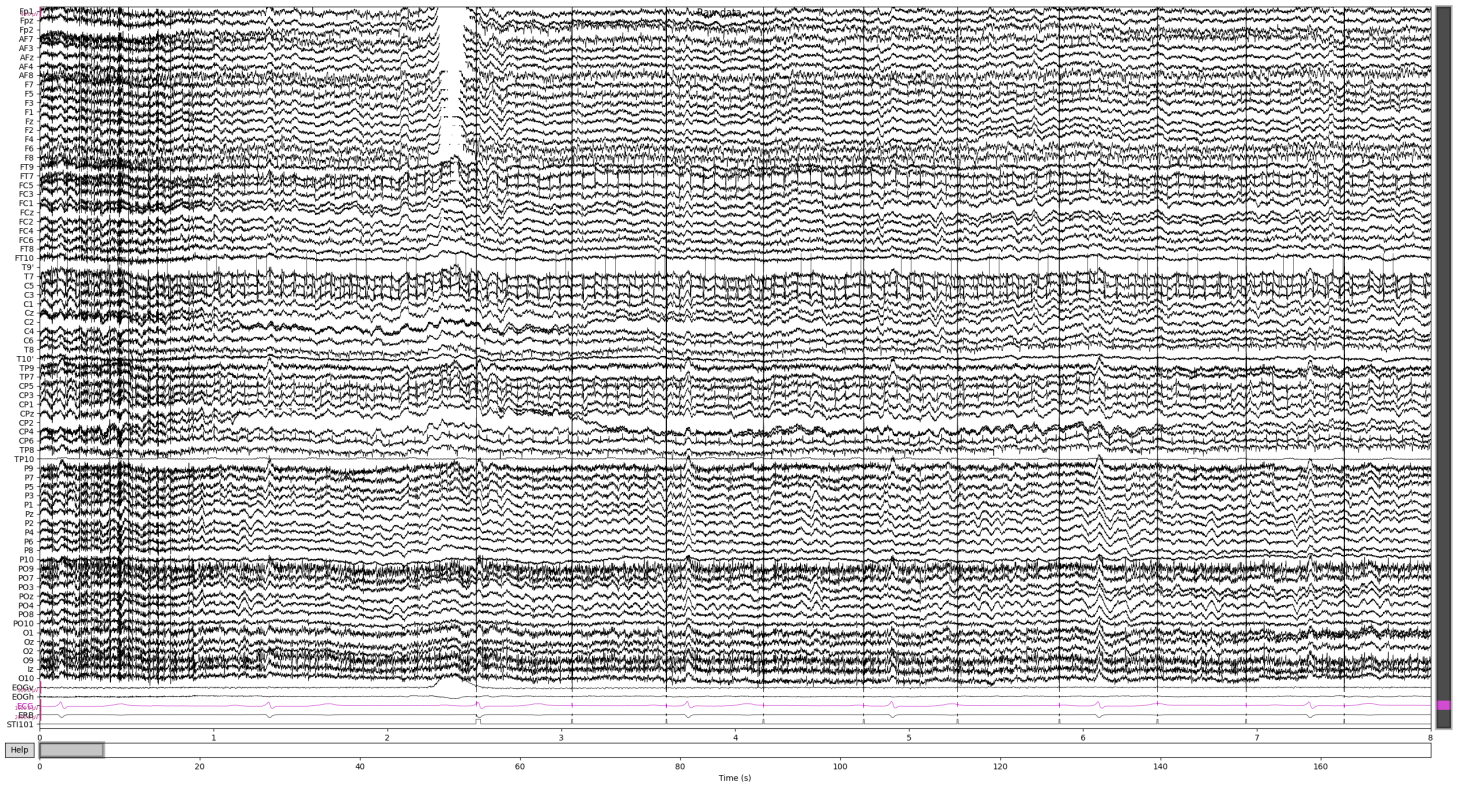


Figure A.1: Plot of the raw EEG signals.

A.2 Filtering

To begin the processing, a filtering step is required, whose results are displayed in Figure A.2, after a notch filter (50, 100 and 150 Hz) and a bandpass filter (between 0.1 and 500 Hz).

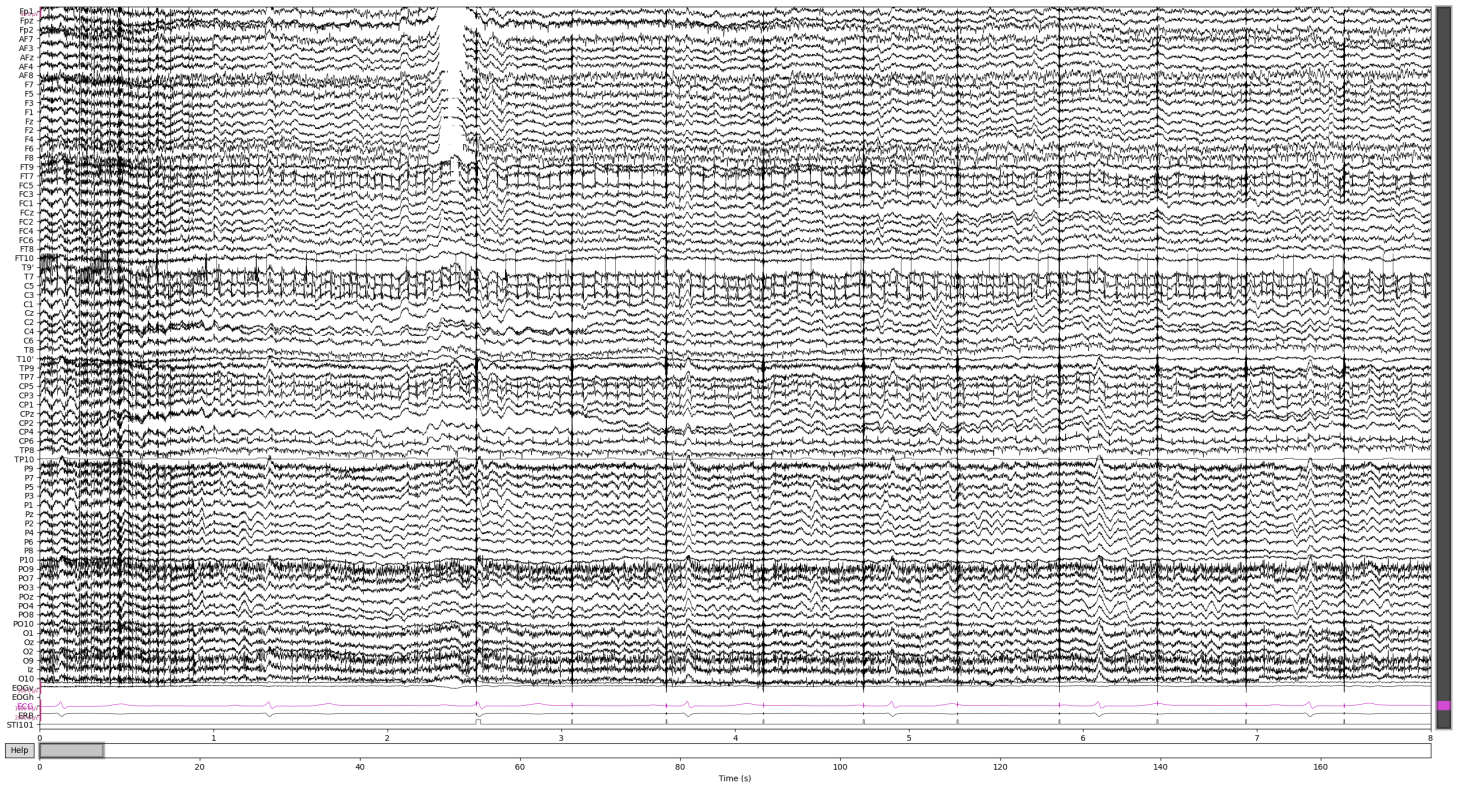


Figure A.2: Plot of the EEG signals after filtering.

A.3 Resampling

Next, to save memory and resources, a resampling is conducted from the original 4000 Hz to merely 1000 Hz (see Figure A.3).

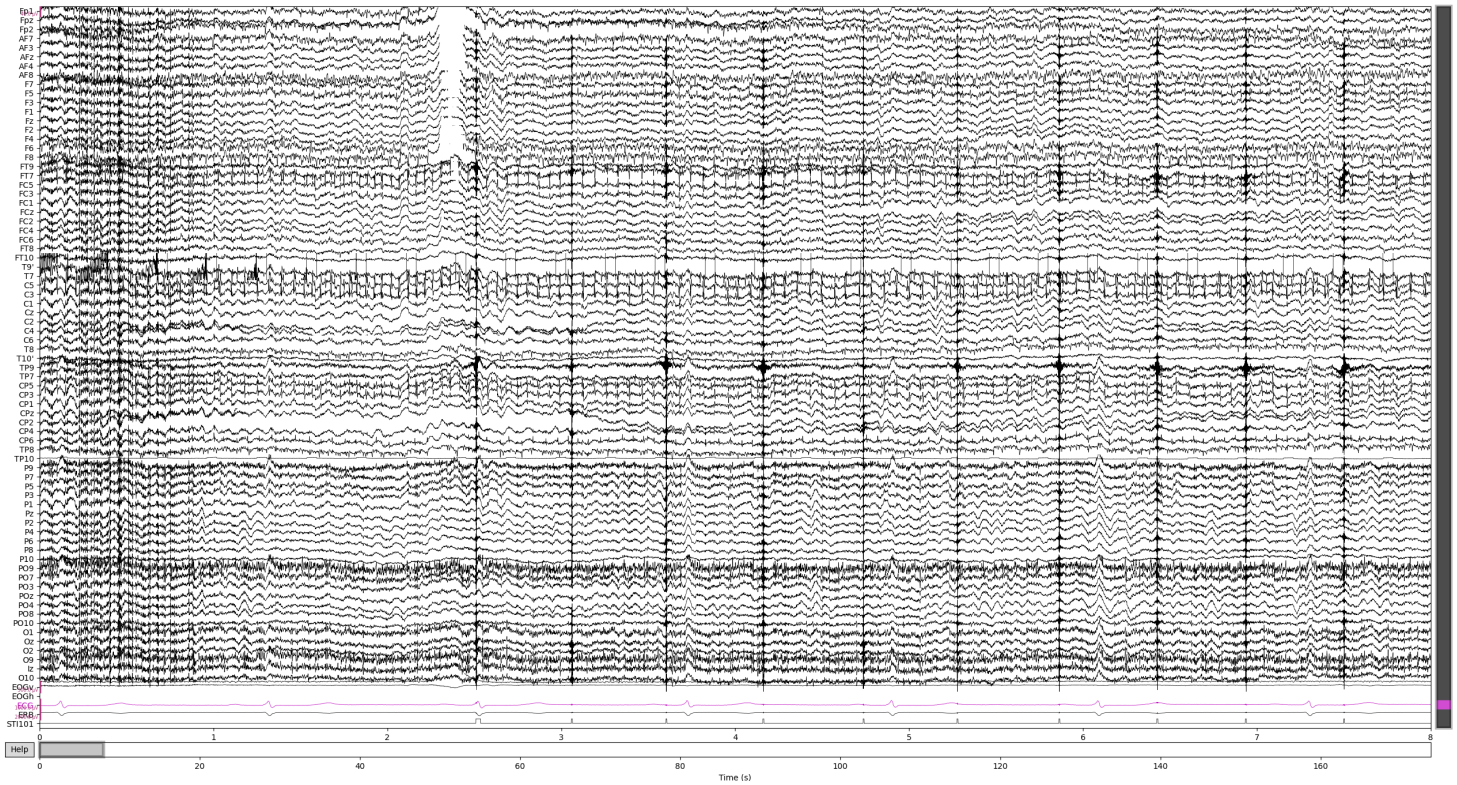


Figure A.3: Plot of the EEG signals after resampling.

A.4 Bad channels

Subsequently, a very important step takes place where bad channels are identified - as illustrated in Figure A.4 - and either interpolated or permanently removed from the recording. When faced with the scenario of having to choose between a lot of bad channels, care was taken during the analysis to try not to interpolate too many channels, as that impacts the subsequent analysis. Instead, the choice was made to interpolate channels within the region of interest and delete channels outside of it. Figure A.5 illustrates the results of an interpolation that is performed once the desired channels have been chosen.

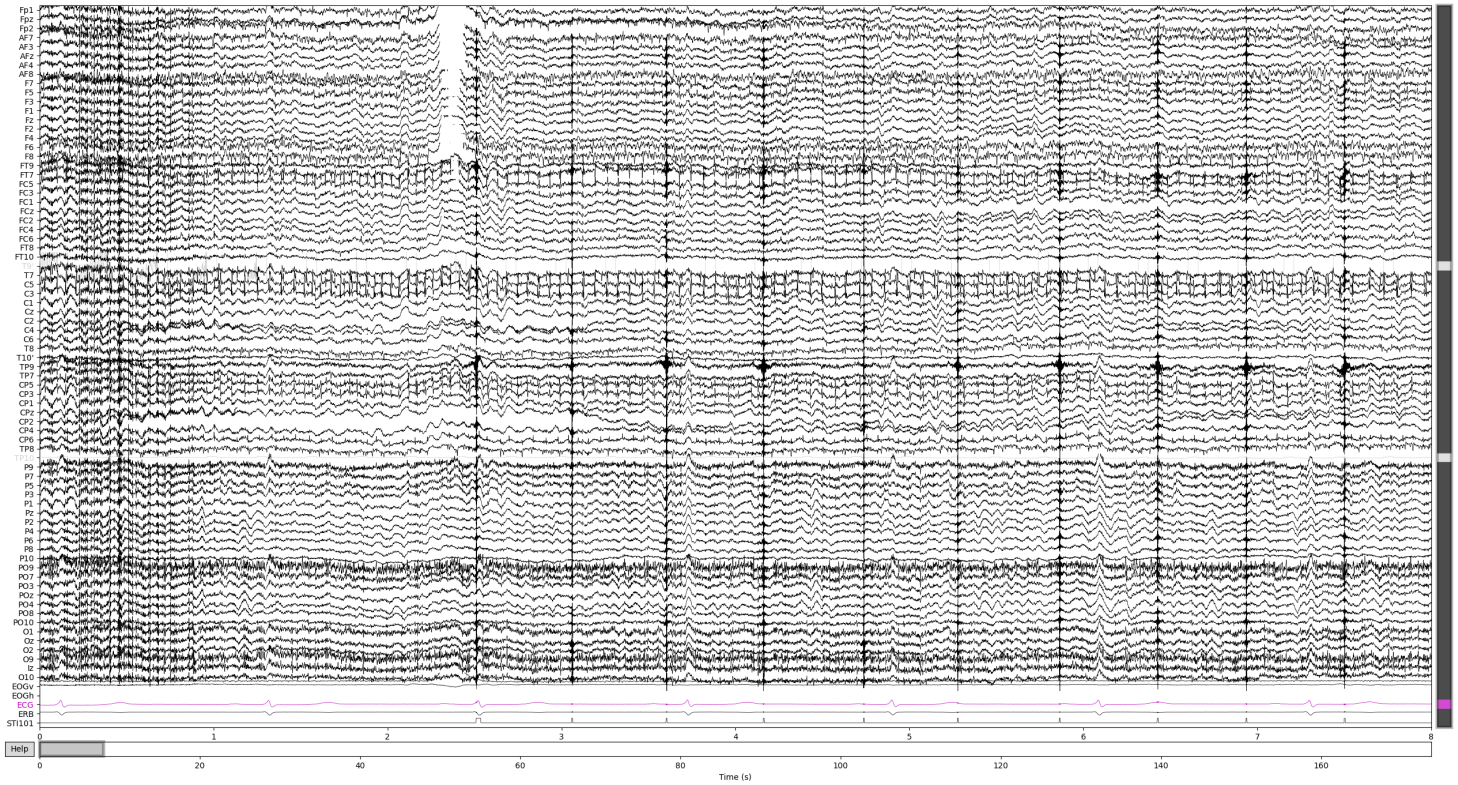


Figure A.4: Plot of the EEG signals after bad channels.

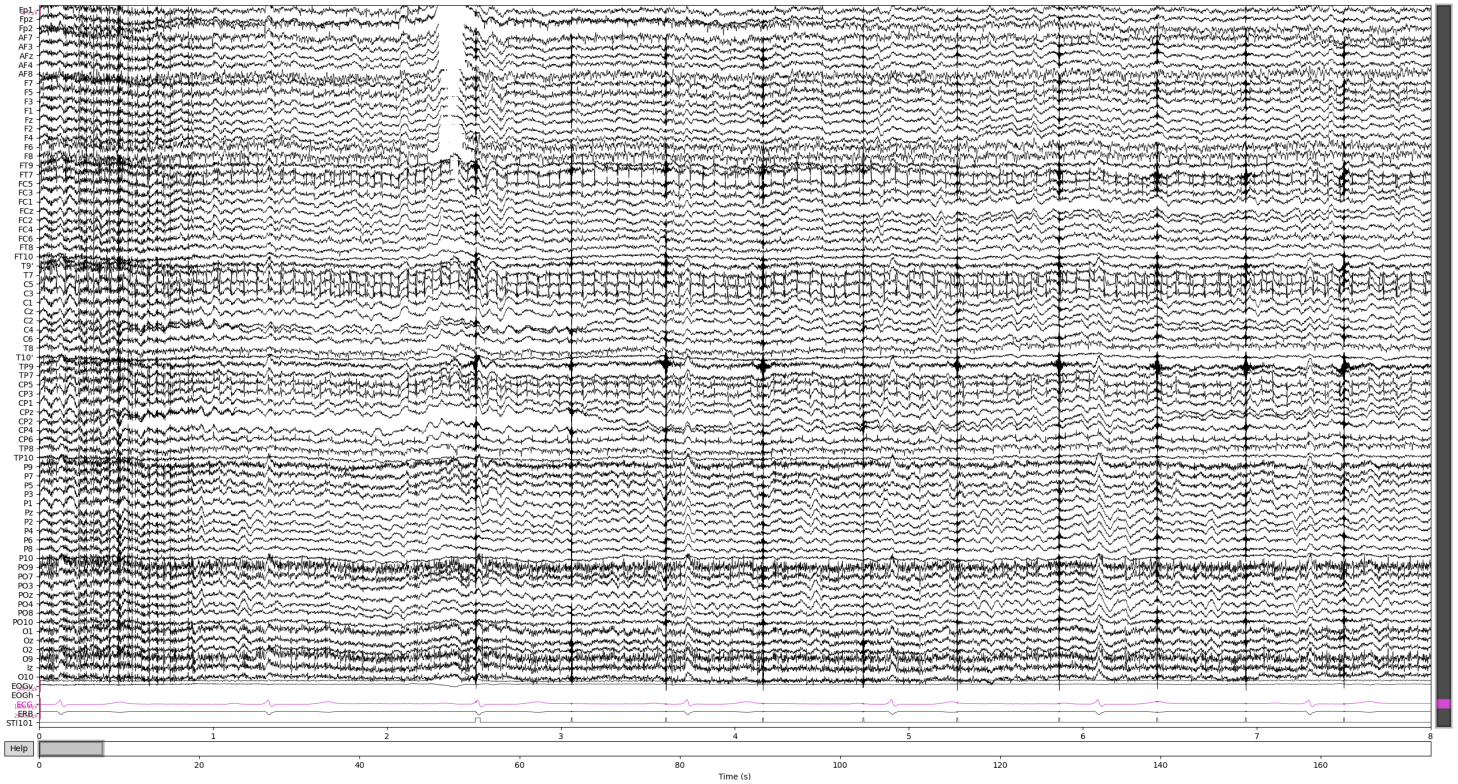


Figure A.5: Plot of the EEG signals after interpolation of bad channels.

A.5 Re-referencing

An average re-referencing stage occurs mainly to improve the quality of the signal (see Figure A.6). Not only does it reduces noise by eliminating common noises across electrodes, but it also balances the signal as each electrode can have a unique baseline or offset. This allows signals to be more comparable across electrodes after re-referencing.

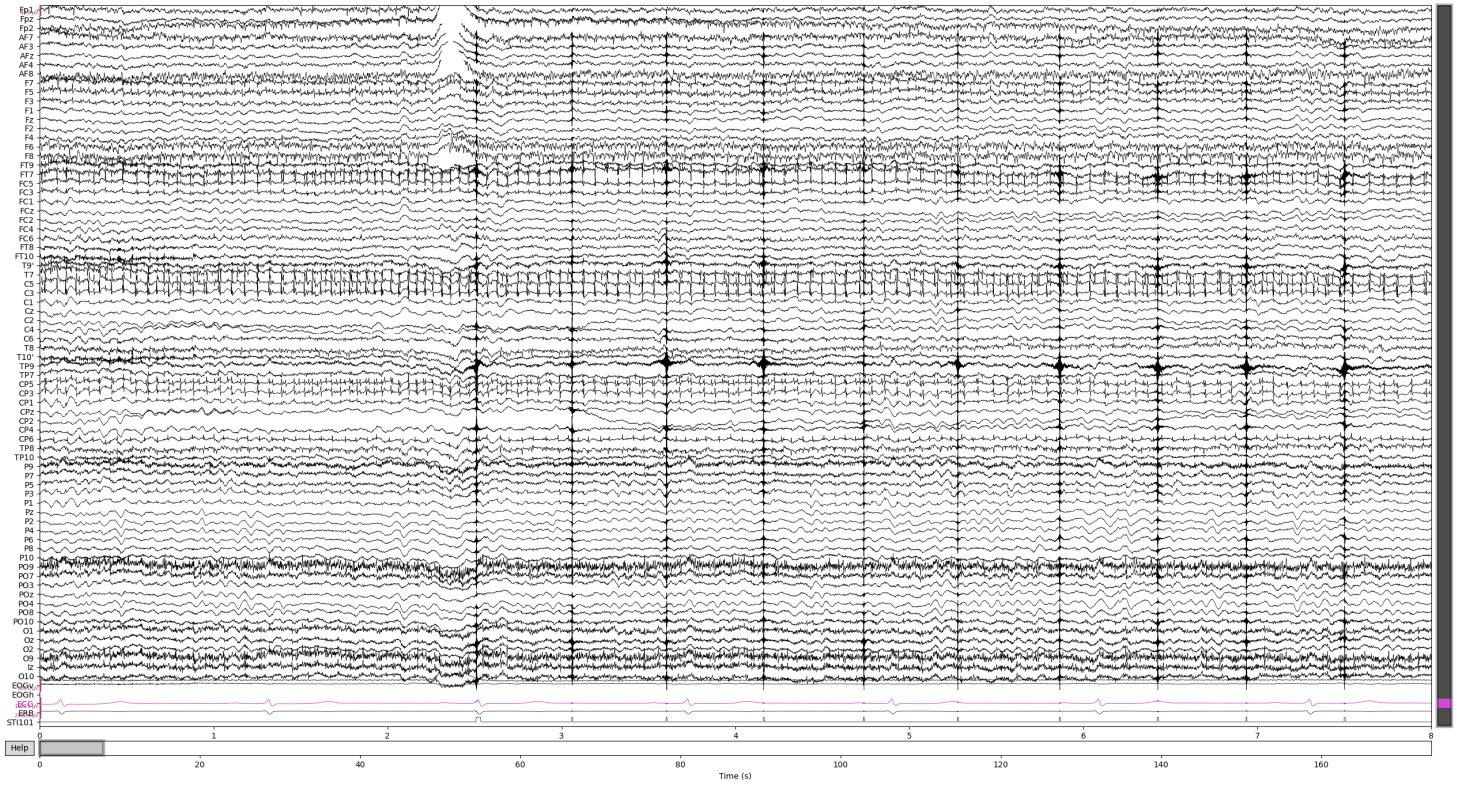


Figure A.6: Plot of the EEG signals after re-referencing.

A.6 ICA

To eliminate artefacts due to muscle, heart beats, eye movements or even bad electrodes, performing an ICA stage is crucial. A total of 70 components was chosen to be considered and the first 20, which represent the 20 biggest sources of signal (neural or not), are displayed in Figure A.7.

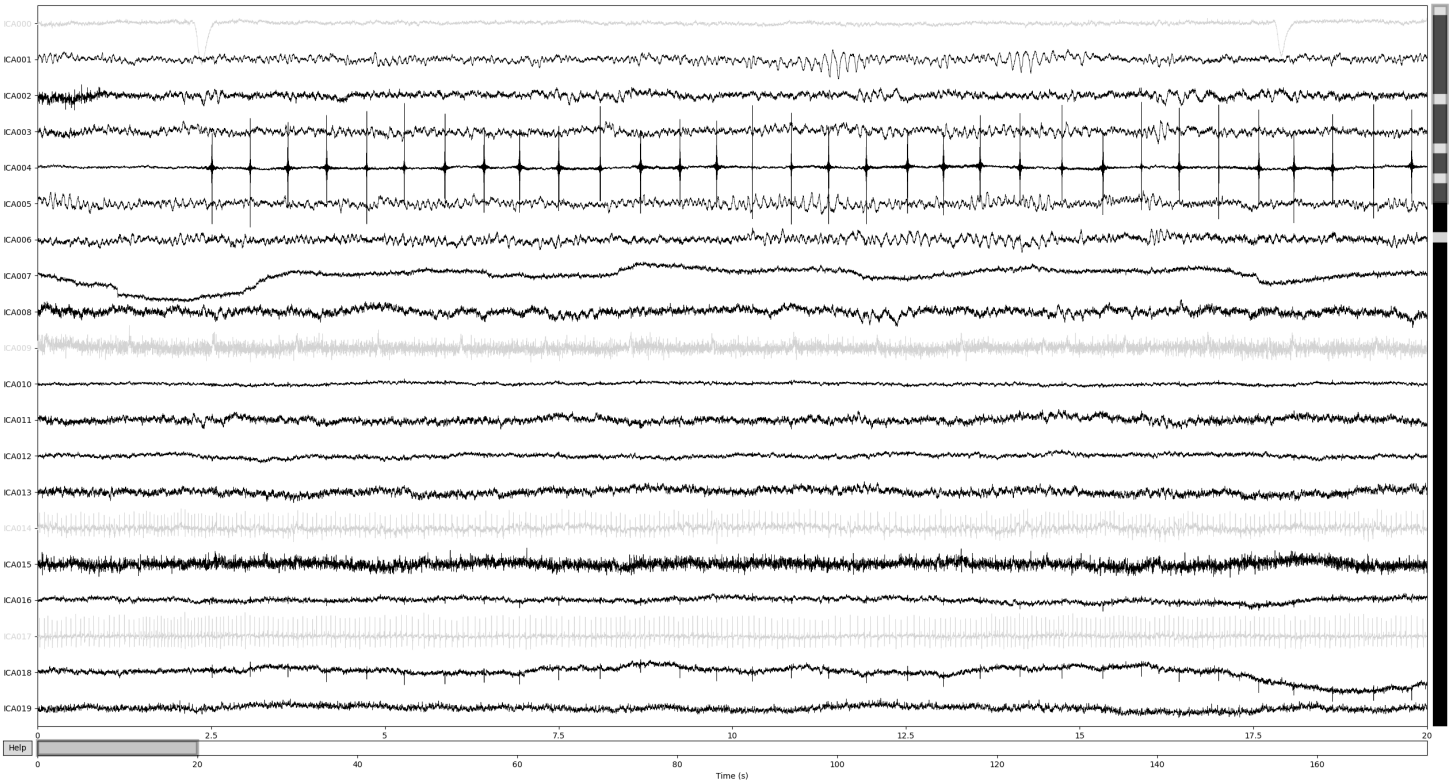


Figure A.7: Plot of the 20 first ICA components.

A topographic map of each component was displayed to aid in the identification of the components that correspond to non-neural signals, providing a visual assessment of the signal's source. Once more, the first 20 components are visible in Figure A.8.

Additionally, it is evident from the two earlier figures that the signals that were manually designated as non-neural are marked in grey. While ICA analysis identifies primary signal sources, not all artefacts can always be eliminated because some may be associated with brain activity. As a result, a conservative strategy is adopted to remove only significant artefacts that have a major impact on signal cleaning.

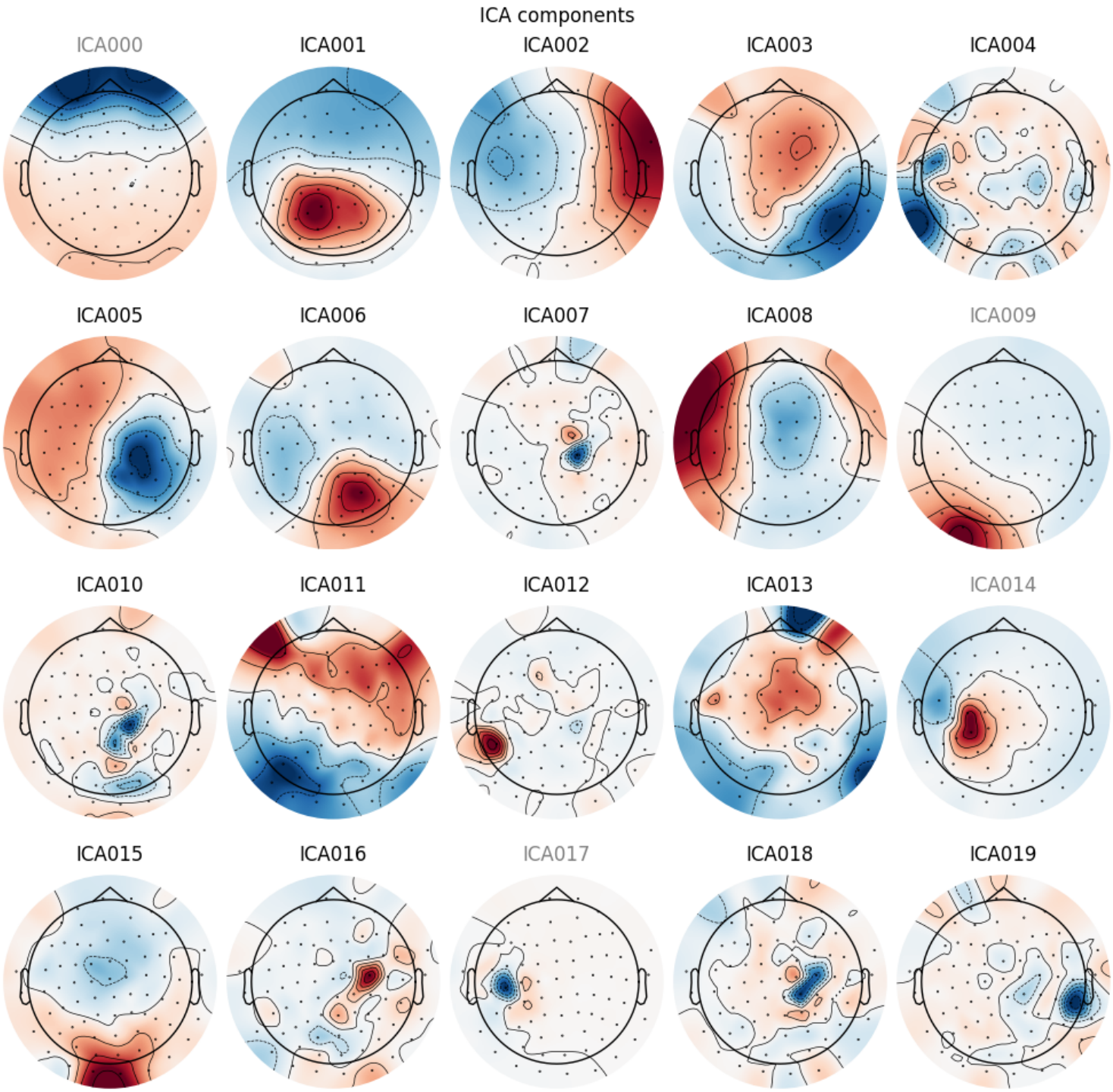
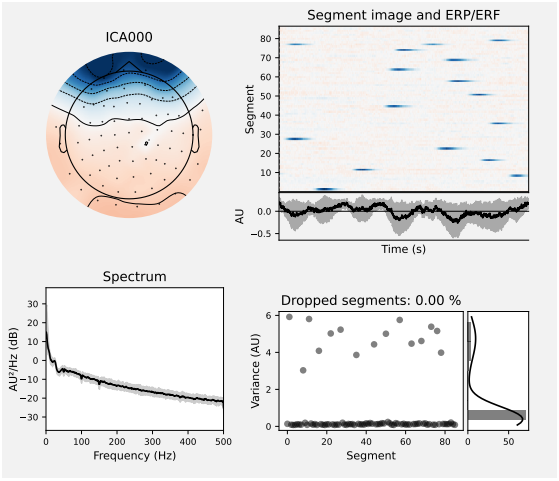
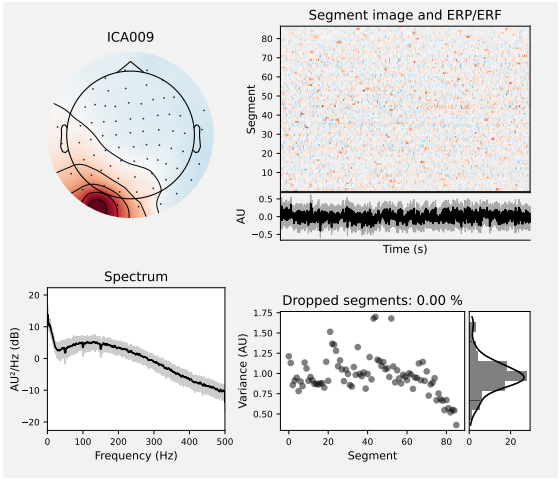


Figure A.8: Plot of the 20 first ICA components topographic maps.

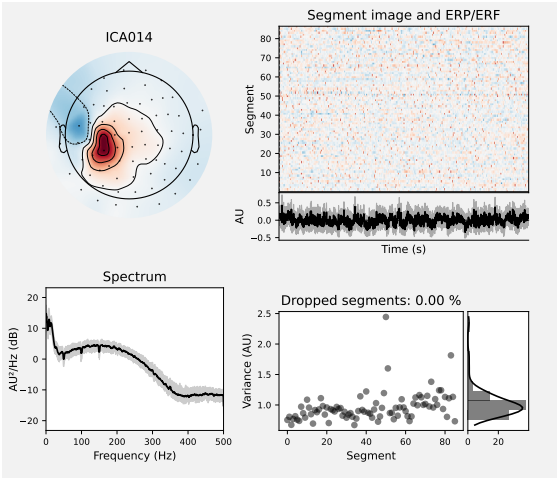
A closer look to the selected components' properties can be seen in Figure A.9.



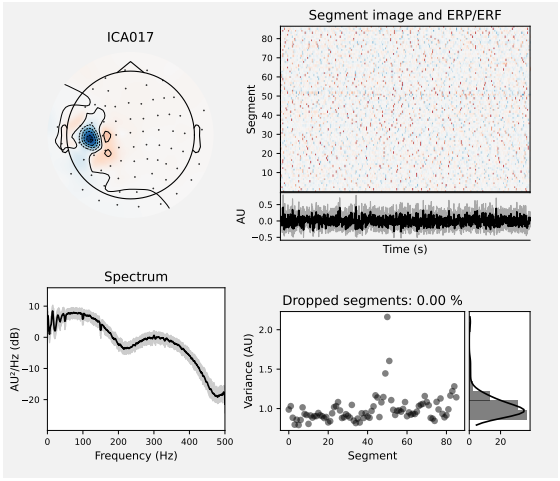
(a) Eye blink.



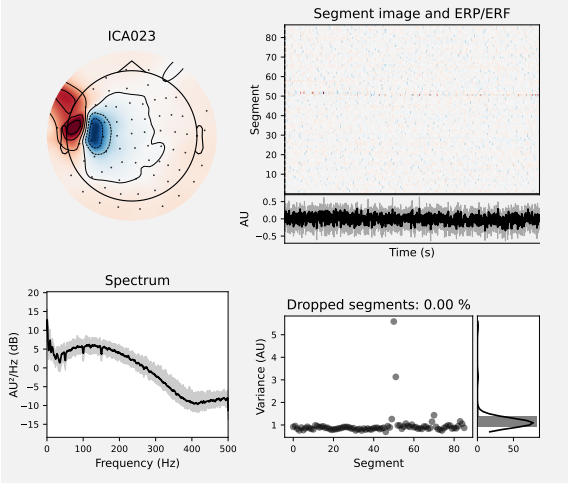
(b) Heart.



(c) Muscle.



(d) Bad electrode.



(e) Muscle.

Figure A.9: ICA artefact components.

A.7 Bad segments

Once the sources of non-neural activity are eliminated from the signal, it is time for a visual and manual selection of bad segments. Bad segments areas are highlighted in red (see Figure A.10), where in this case mainly frontal channels are noisy, probably due to head movements. Once registered, bad segments will be removed from the signal and not taken into consideration for the last step of preprocessing.

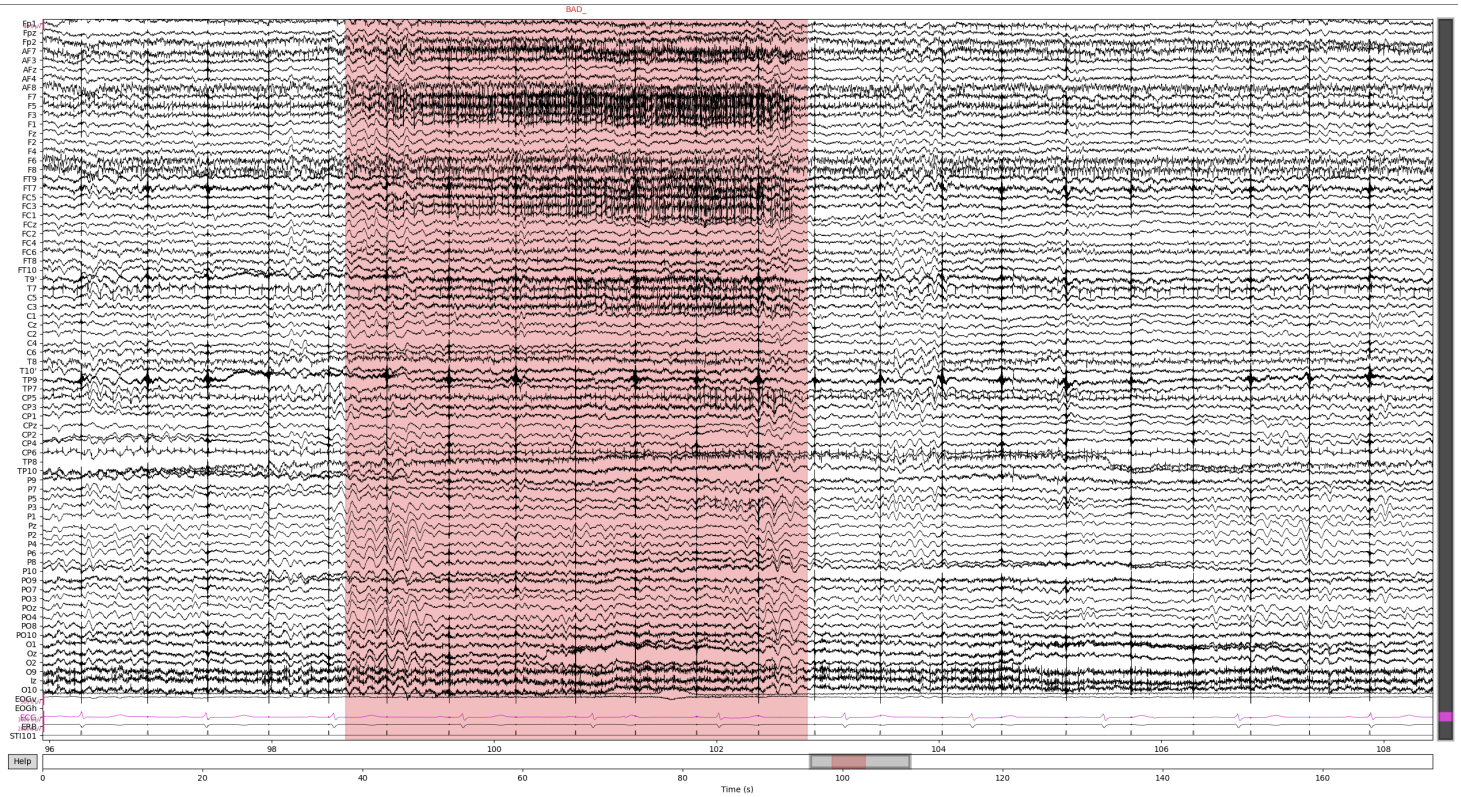


Figure A.10: Plot of the EEG signals marking bad segments.

A.8 Epochs

Ultimately, once all data has been clean from noise and artefacts it is time to segment the time series into epochs of 500 ms around the triggered sensory stimuli. This step is shown in Figure A.11 where, if necessary, it is still possible to select epochs that present anomalies to be eliminated.

After all the above mentioned stages, the signal is ready to be analysed by the desired methods.

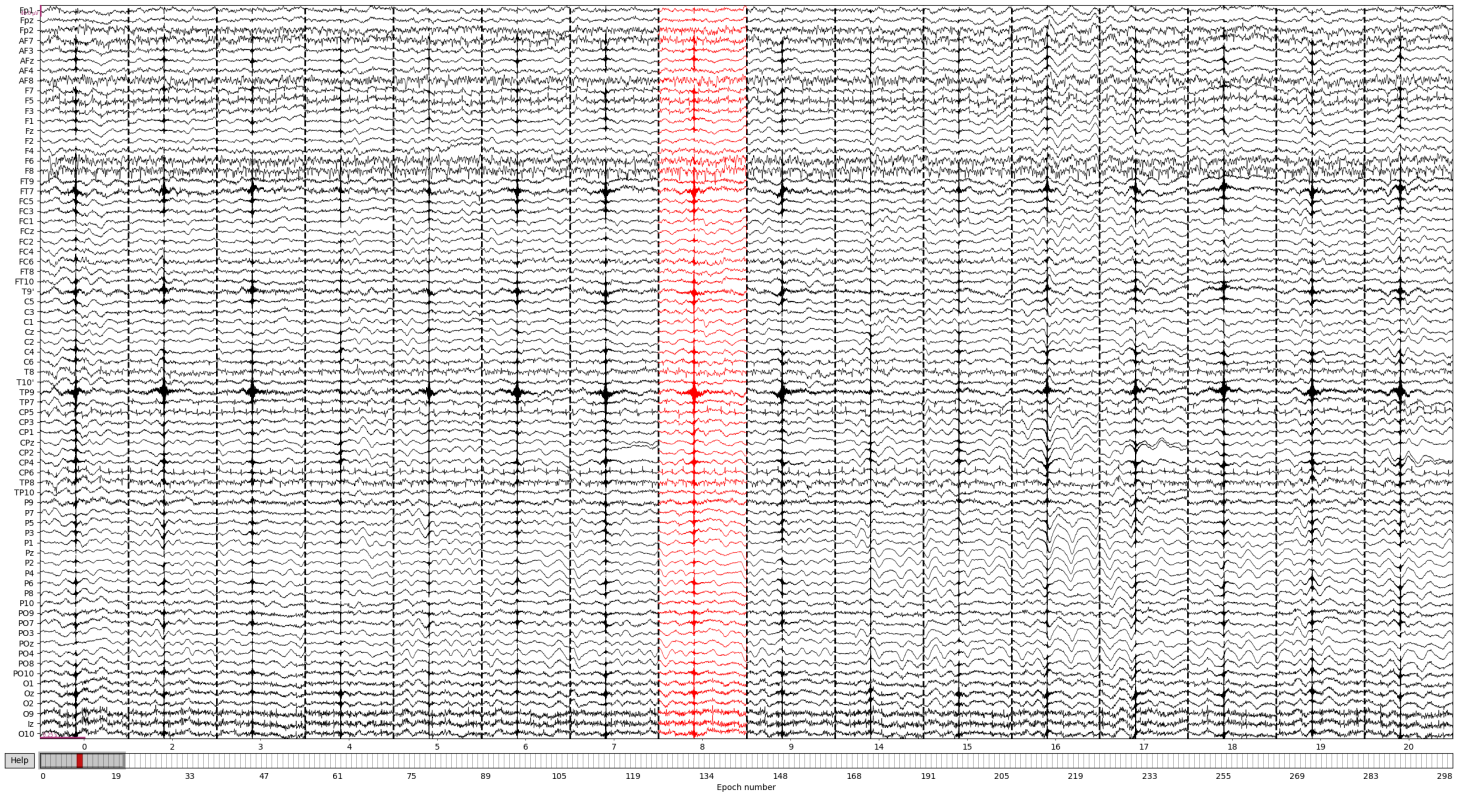


Figure A.11: Plot of the EEG signals after epoching.

B

Preprocessing filters' frequencies

In order to properly establish the cut-off frequencies for both the Notch and bandpass filters employed during preprocessing, two small analyses were carried out, the details of which are provided in the following sections.

B.1 Data spectrum analysis

For the Notch filter, the spectrum of the raw data was analysed, as seen in Figure B.1. From here, and after a visual inspection, it was decided to select the two first harmonics of the powerline interference besides the powerline noise frequency itself, ie, 50, 100 and 150 Hz. A filtered data spectrum was generated (see Figure B.2) to confirm the selection and accurate removal of certain frequencies, hence validating the use of the Notch filter.

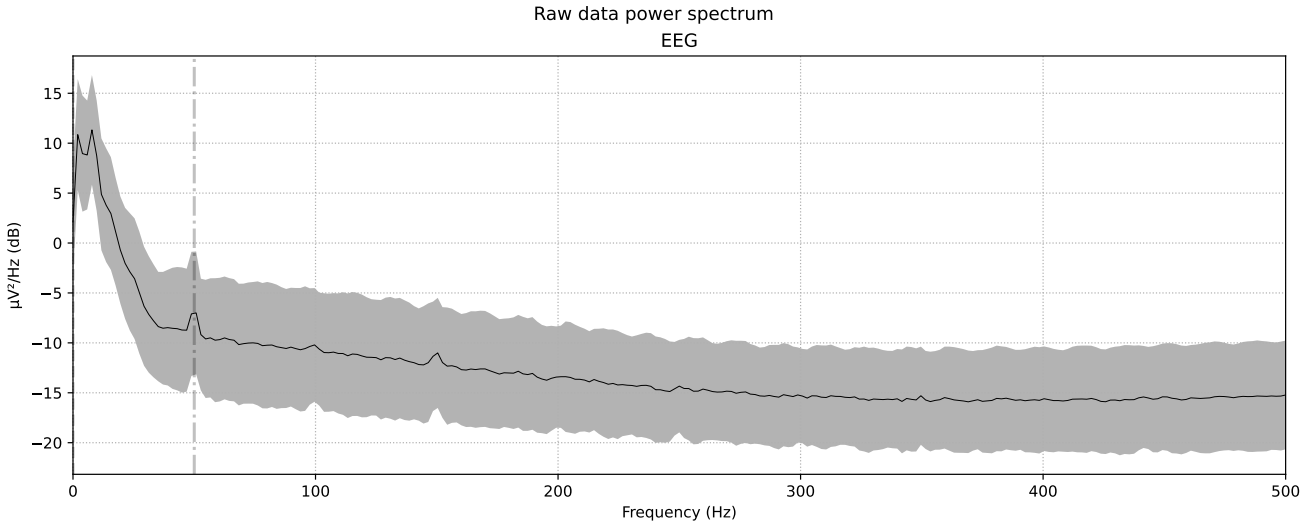


Figure B.1: Plot of the power spectrum data of raw EEG signals.

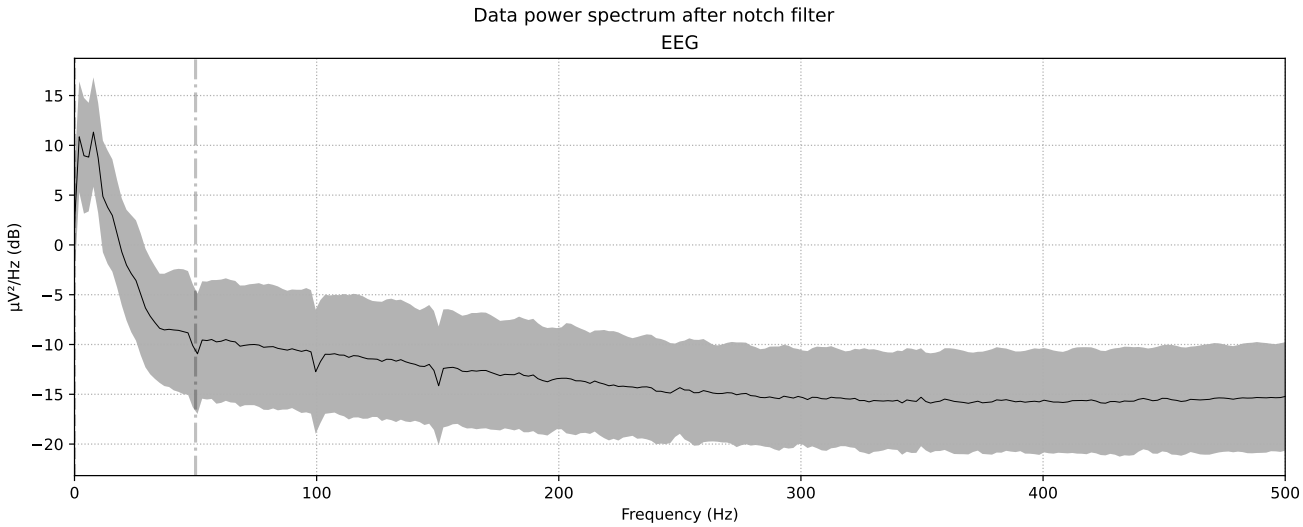
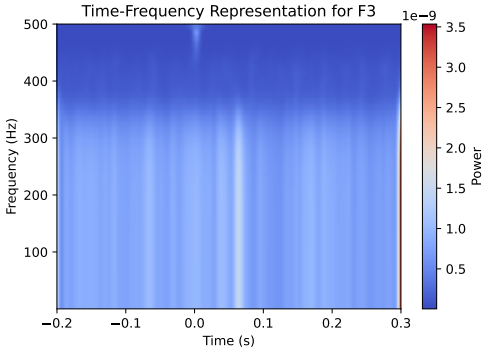


Figure B.2: Plot of the power spectrum data after filtering the EEG.

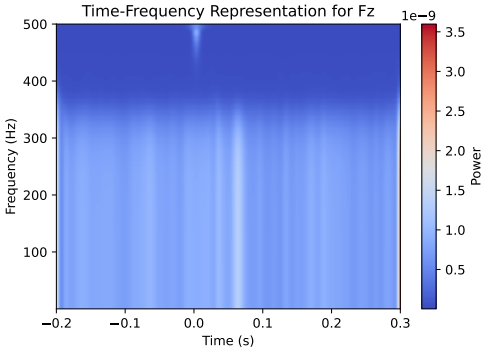
B.2 Time frequency analysis

Each channel underwent a temporal frequency analysis to determine the frequencies at which important activity stopped occurring. After closely reviewing each plot and paying particular attention to channels of interest (see Figure B.3), it was evident that there was essentially no activity starting from 400 Hz. Thus, for the low-pass filter a cut-off frequency of 500 Hz was chosen.

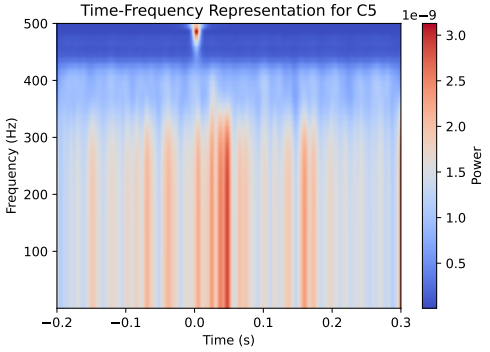
Regarding the high-pass cutoff frequency, the value of 0.1 Hz was chosen based on literature [57].



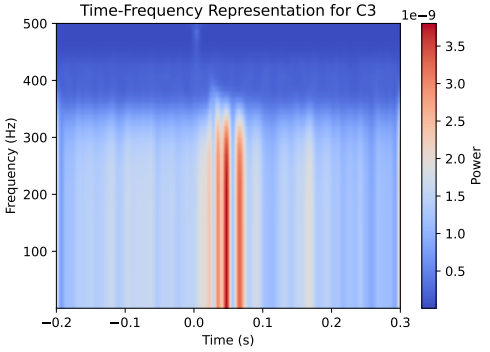
(a) F3.



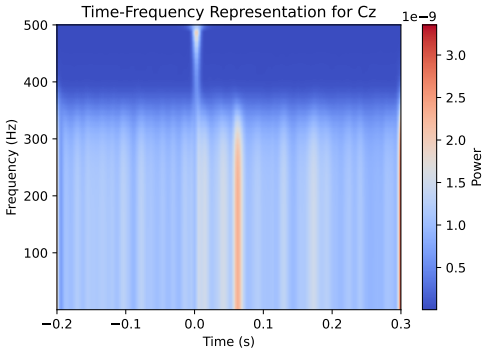
(b) Fz.



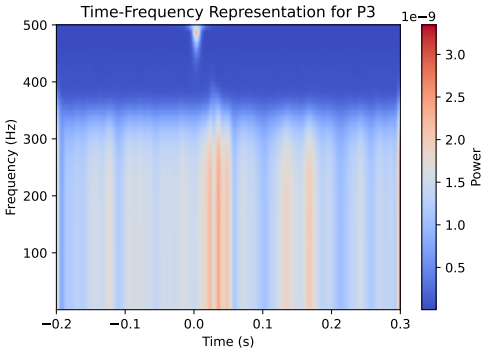
(c) C5.



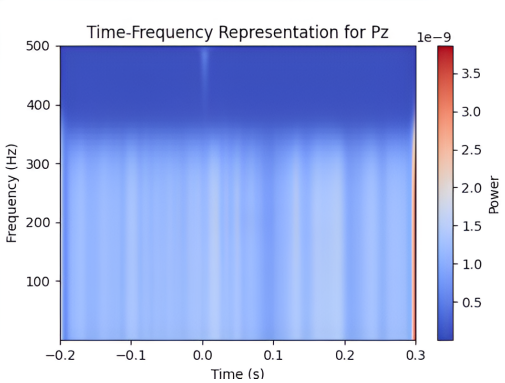
(d) C3.



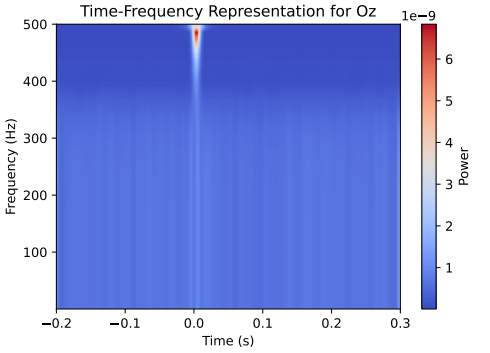
(e) Cz.



(f) P3.



(g) Pz.



(h) Oz.

Figure B.3: Time frequency analysis on channels of interest.

C

MI calculus steps

In this work, the MI used to detect CFC between frequency ranges of interest followed the methodology developed by Tort [26]. Accordingly, the steps to compute it are the following:

1. The raw signal, $x_{raw}(t)$, is filtered at phase, $x_{f_p}(t)$, and amplitude, $x_{f_A}(t)$ (frequency ranges of interest, f_p and f_A).

2. Phase and amplitude time series, $\phi_{f_p}(t)$ and $A_{f_A}(t)$, are calculated from the raw signal using the Hilbert transform. A composite phase-amplitude time series is constructed, $[\phi_{f_p}(t), A_{f_A}(t)]$ which informs the amplitude of the f_A oscillation at each phase of the f_p rhythm.

3. The referred composite time series ($\phi_{f_p}(t)$) is used to calculate the mean amplitude distribution over 18 20° phase bins. $\langle A_{f_A} \rangle_{\phi_{f_p}}(j)$ represents the mean A_{f_A} value for each phase bin j.

4. Entropy measure H is applied: $H = -\sum_{j=1}^{N=18} p_j \log(p_j)$, where p_j is defined by

$$p_j = \frac{\langle A_{f_A} \rangle_{\phi_{f_p}}(j)}{\sum_{j=1}^{N=18} \langle A_{f_A} \rangle_{\phi_{f_p}}(j)}.$$

5. The MI is ultimately obtained by normalizing H by the highest entropy value H_{max}, which is achieved for the uniform distribution $p_j = 1/N$ (and hence $H_{max} = log(N)$:

$$MI = \frac{H_{max} - H}{H_{max}}.$$

These above mentioned steps are illustrated in the Figure C.1 below.

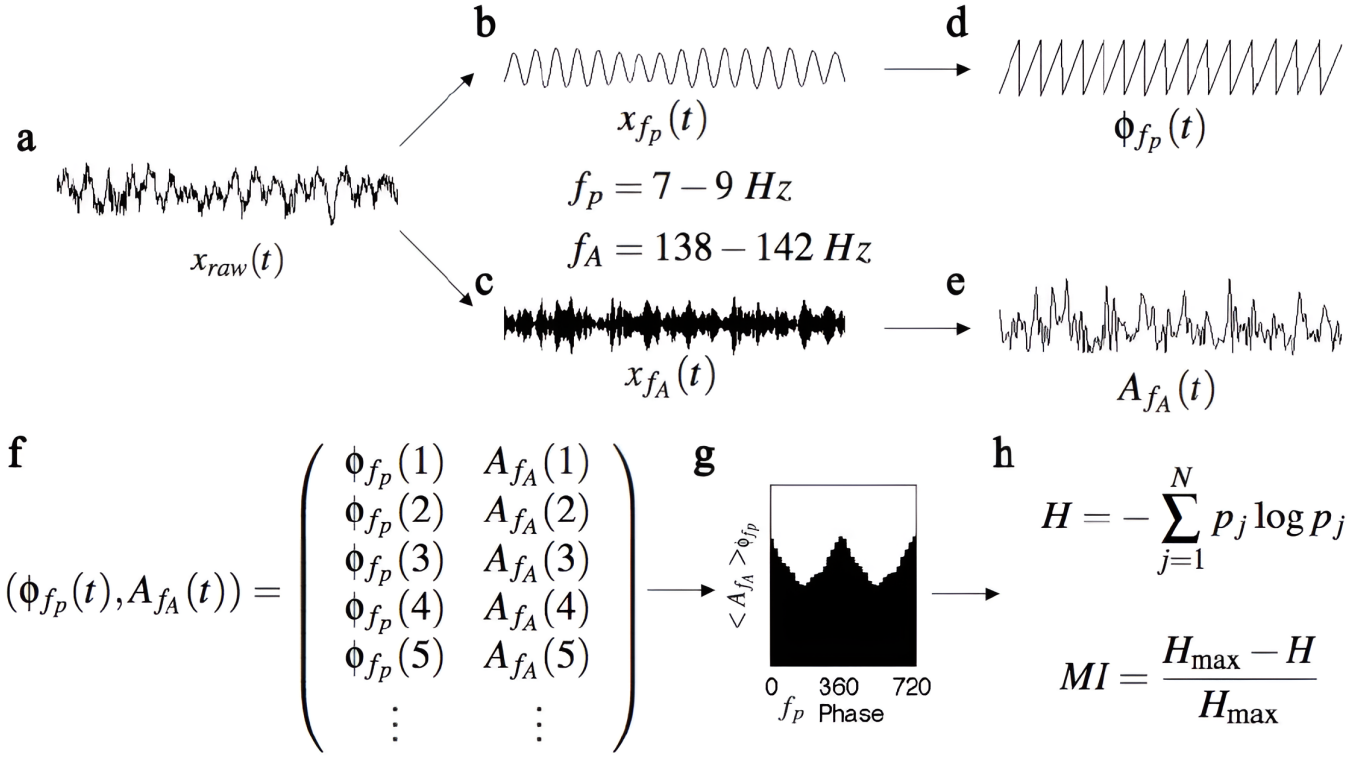


Figure C.1: Steps in the computation of the MI. **(a-c)** The raw signal (a) is filtered at the desired frequency ranges for phase (b) and amplitude (c). **(d, e)** The Hilbert transform is then used to calculate the phase (d) and amplitude (e) time series from the filtered signals. **(f, g)** A composite time series (f) is built and utilised to determine the mean amplitude values at each 20º phase bin (g). **(h)** Using a normalised entropy measure on the mean amplitude vector, the MI is ultimately derived. Reproduced with permission from [26], Copyright (2008) National Academy of Sciences.

D

Linear Mixed model specifications

The chosen model to perform statistical analysis was a repeated measures (full factorial design) linear mixed effect model, and it was constructed with JMP®. The factorial repeated measures design examines experimental procedures in which several measurements are performed on the same individuals and one or two factors distinguish the subjects; it involves a complete cross of factors.

For the construction of the model factors had to be decided, as illustrated by Figure D.1.

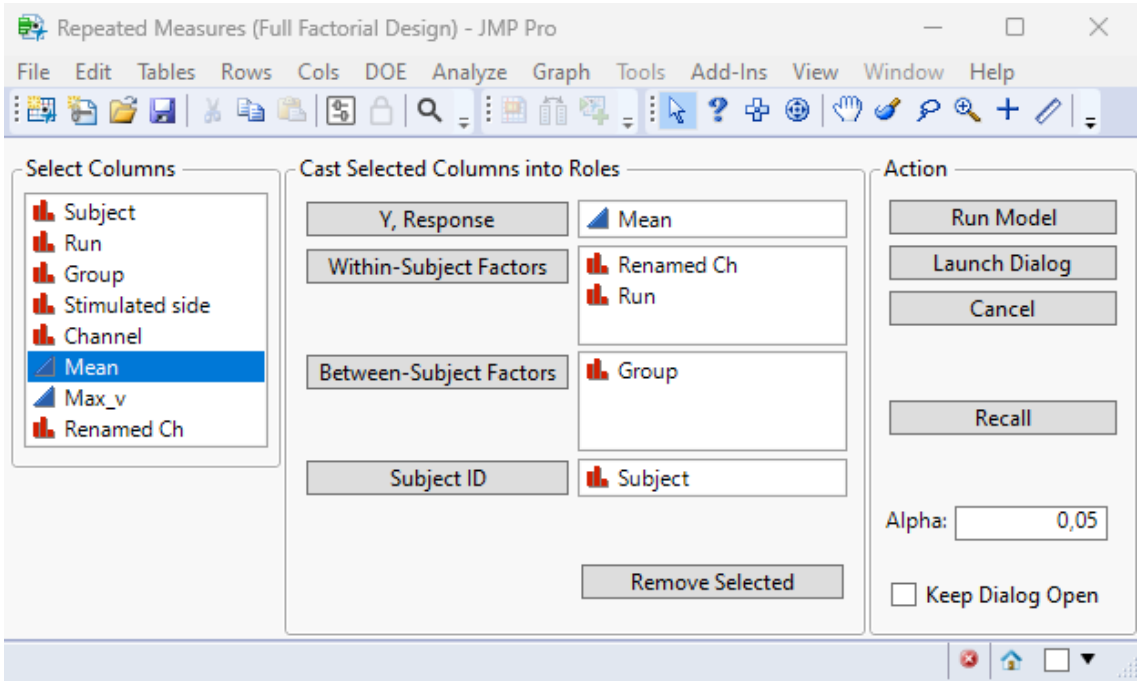


Figure D.1: Linear mixed model menu.

The "Y, response" is the parameter we are interested in studying when constructing the model, therefore the choice of the mean. A "within-subject" factor is a factor that can have multiple existences for the same subject, as it is the case of Channel (74 per subject) and Run (1 or 2, when existent). "Between-subject" factors are the ones where a subject can

only be measure at one level, such as Group (either control or ALS, but not both). Finally, "subject ID" refers to the identification of each subject in the dataset that is provided to the model.

